UNIVERSITY OF ZAGREB
FACULTY OF MECHANICAL ENGINEERING
AND NAVAL ARCHITECTURE

MASTER'S THESIS

Jakov Baleta

Zagreb, 2013

SVEUČILIŠTE U ZAGREBU
FAKULTET STROJARSTVA I BRODOGRADNJE

DIPLOMSKI RAD

Jakov Baleta

Zagreb, 2013.

UNIVERSITY OF ZAGREB
FACULTY OF MECHANICAL ENGINEERING
AND NAVAL ARCHITECTURE

NUMERICAL INVESTIGATION OF WALLFILM FORMATION FOR SELECTIVE CATALYTIC REDUCTION APPLICATIONS

Supervisors:

Prof. dr. sc. Neven Duić, dipl. ing.

Student:

Jakov Baleta

Zagreb, 2013

SVEUČILIŠTE U ZAGREBU
FAKULTET STROJARSTVA I BRODOGRADNJE

NUMERIČKA ANALIZA STVARANJA FILMA TEKUĆINE NA STIJENCI ZA PRIMJENU U SELEKTIVNOJ KATALITIČKOJ REDUKCIJI

Mentori: Student:

Prof. dr. sc. Neven Duić, dipl. ing. Jakov Baleta

Zagreb, 2013.

I hereby declare that this thesis is entirely the result of my own work and knowledge obtained during my studies, except where otherwise indicated. I have fully cited all used sources and I have only used the ones given in the list of references.

I would like to begin expressing my gratitude to my supervisor, Professor Neven Duić for giving me this great opportunity to participate in international collaboration with AVL List GmbH. Financial support for this work is gratefully acknowledged from AVL Croatia and its manager mr. sc. Goran Mirković.

I am also grateful to Dr. Klaus Pachler for valuable advices, discussions and guidance throughout this work.

Special thanks to Dr. Milan Vujanović for his advices, guidance, patience and support. His inexhaustible positive energy and bright personality kept me motivated during the hardest periods of making this work.

I would also extend my appreciation to guys from PowerLab for their technical support.

Finally and most important, I am truly thankful to my family for their unconditional love, understanding, patience and support. I was very strenuous person during the final period of my study and you managed not only to put up with me but also give me strength and hope into favorable outcome. Unforunatelly, not all were able to live long enough to see the end of my education. To them I dedicate this work.

Jakov Baleta, May 14th, 2013

SVEUČILIŠTE U ZAGREBU
FAKULTET STROJARSTVA I BRODOGRADNJE
Središnje povjerenstvo za završne i diplomske ispite
Povjerenstvo za diplomske ispite studija strojarstva za smjerove:
procesno-energetski, konstrukcijski, brodostrojarski i inženjersko modeliranje i računalne simulacije

Sveučilište u Zagrebu Fakultet strojarstva i brodogradnje	
Datum	Prilog
Klasa:	
Ur.broj:	

DIPLOMSKI ZADATAK

Student: **Jakov Baleta** Mat. br.: **0035167604**

Naslov rada na hrvatskom jeziku: **Numerička analiza stvaranja filma tekućine na stijenci za primjenu u selektivnoj katalitičkoj redukciji**

Naslov rada na engleskom jeziku: **Numerical investigation of wallfilm formation for selective catalytic reduction applications**

Opis zadatka:

Selektivna katalitička redukcija bazirana na vodenoj otopini uree je trenutno najperspektivnija metoda za ispunjavanje strogih zahtjeva nadolazeće Euro 6 norme na NOx emisije iz diesel motora. Nakon što se vodena otopina uree u obliku spreja ubrizga u struju vrućih dimnih plinova prije katalizatora, dolazi do isparavanja vode iz otopine i stvaranja amonijaka termalnom dekompozicijom uree i hidrolizom izocijanske kiseline. Nastali amonijak sudjeluje u različitim deNOx reakcijama kao reducirajuće sredstvo. Rezultirajuća prostorna raspodjela amonijaka prije katalizatora je ključni faktor učinkovite konverzije NOx-a. Na nju, uz procese isparavanja i dekompozicije, također utječe i interakcija spreja i stijenke.

Zadatak ovog diplomskog rada je istraživanje interakcije spreja s vrućom zračnom strujom i stijenkom uz pomoć numeričke simulacije i validacija matematičkih modela integriranih u komercijalni CFD kod „Fire".

U okviru diplomskog zadatka potrebno je:
1. Upoznati se s programskim paketom „Fire Workflow Manager" i Lagrangeovom višefaznom metodom.
2. Izvršiti kalibraciju spreja uz pomoć dostupnih eksperimentalnih podataka.
3. Korištenjem komercijalnog programskog paketa „Fire Workflow Manager" napraviti detaljnu 3D numeričku simulaciju na domeni koju čini pravokutni kanal dimenzija 970 x 120 x 45 mm.
4. Provesti analizu rezultata.
5. Dobivene simulacijske rezultate je potrebno usporediti s postojećim eksperimentalnim podacima kako bi se provjerila njihova točnost.

Svi ulazni podaci potrebni za izračun i provođenje ovog zadatka mogu se dobiti kod mentora.

U diplomskom radu potrebno je navesti svu upotrebljenu literaturu i eventualnu pomoć pri izradi rada.

Zadatak zadan:	Rok predaje rada:	Predviđeni datumi obrane:
14. ožujka 2013.	16. svibnja 2013.	22. - 24. svibnja 2013.

Zadatak zadao:

Prof. dr. sc. Neven Duić

Predsjednik Povjerenstva:

Prof. dr. sc. Zvonimir Guzović

CONTENTS

LIST OF FIGURES

LIST OF TABLES

NOMENCLATURE

Roman	Unit	Description
A	kg/(s·m)	frequency rate
B_T	-	heat transfer number
B_Y	-	mass transfer number
$\bar{c}_{pF}$	J/(kg·K)	specific heat capacity of the vapour
C	-	model constant
C_b	-	dimensionless constant in secondary break-up model
C_d	-	dimensionless constant in secondary break-up model
C_F	-	dimensionless constant in secondary break-up model
C_k	-	dimensionless constant in secondary break-up model
d	m	nozzle exit diameter
$D90$	μm	statistical characteristic of spray
d_d	m	droplet diameter
D_d	μm	droplet diameter
D_{mean}	μm	arithmetic mean of particle sizes
dp/dx	Pa/m	pressure gradient
d_t	m	tube diameter
d_{zp}	m	wall distance
E_a	J/mol	activation energy
$F(B)$	-	film thickness correction function
F_{ib}	N	sum of other external forces
F_{idr}	N	drag force
F_{ig}	N	force including effects of gravity and buoyancy
F_{ip}	N	pressure force
F_M	-	diffusional film correction factor
F_T	-	diffusional film correction factor
g	m/s^2	gravitational acceleration
h	m	liquid height
i	J/kg	specific internal energy
K	-	dimensionless droplet velocity
k	W/(m·K)	thermal conductivity
k_s	m	the equivalent sand grain roughness
$\bar{k}_g$	W/(m·K)	thermal conductivity of the gas mixture at reference conditions
Le	-	Lewis number
$\dot{m}$	kg/s	droplet evaporated mass flow
m_d	kg	droplet mass

$\dot{m}_{vap}$	kg/s	mass flow of evaporated liquid
M_i	g/mol	molar mass of ith species
Nu^*	-	modified Nusselt number
Nu_0	-	Nusselt number of the non-evaporating droplet
Oh	-	Ohnesorge number
p	Pa	pressure
Pr	-	Prandtl number
Q_s	J	heat transferred to droplet
r	m	droplet radius
R	J/(mol·K)	universal gas constant
Re	-	Reynolds number
Re_{ks}	-	Reynolds number for roughness
Sc	-	Schmidt number
Sh^*	-	modified Sherwood number
Sh_0	-	Sherwood number of a non-evaporating droplet
S_i	W/m^3	heat source
S_{mD}	kg/s	source term
S_{mdt}	μm	Sauter mean diameter
S_{mV}	kg/s	source term
S_{mx}	N/m^3	x momentum source
S_{my}	N/m^3	y momentum source
S_{mz}	N/m^3	z momentum source
S_ϕ	-	general source term
t	s	time
T	K	temperature
T^*	-	dimensionless temperature
$\bar{T}$	K	reference temperature
T_s	K	droplet saturation temperature
T_w	K	wall temperature
u	m/s	x velocity component
$\boldsymbol{u}$	m/s	velocity vector
$u_{//}$	m/s	wall parallel velocity
u_1	m/s	film velocity component
u_2	m/s	film velocity component
$u_{d\perp}$	m/s	wall normal component of droplet velocity
u_{id}	m/s	droplet velocity
$\bar{u}_L$	m/s	mean film velocity for laminar flow
$\bar{u}_T$	m/s	mean film velocity for turbulent flow
u_τ	m/s	friction velocity
v	m/s	y velocity component

V	m^3	volume
V_{lmean}	μm	mean of cubes of particle diameters
w	m/s	z velocity component
We	-	Weber number
x	m	coordinate direction
x_i	-	mass fraction of ith species
x_{id}	m	location vector
y	m	location coordinate
y	-	displacement of the equator of the droplet from its equilibrium position
y^+	-	dimensionless wall distance
y_i	-	molar fraction of ith species
y_u	-	urea concentration
$\bar{Y}_S$	-	reference vapour concentration
Y_V	-	vapour mass fraction

Greek	**Unit**	**Description**
$\bar{\beta}_g$	m^2/s	binary diffusion coefficient of the gas mixture at reference conditions
Γ	-	general diffusion coefficient
δ_m	m	fictional gas film thickness for mass transfer
δ_T	m	fictional gas film thickness for heat transfer
κ	-	model constant
μ	Pas	dynamic viscosity
μ_d	Pas	dynamic viscosity of droplet
ρ	kg/m^3	liquid density
ρ_d	kg/m^3	density of droplet
ρ_g	kg/m^3	gas density
$\bar{\rho}_g$	kg/m^3	density of the gas mixture at reference conditions
σ	N/m	surface tension
σ_d	N/m	surface tension of droplet
τ_I	N/m^2	shear stress at the phase interface
τ_w	N/m^2	frictional resistance to the air flow
Φ	W/m^3	dissipation function
ϕ	-	general variable
ψ_τ	-	correction function

SUMMARY

The urea-water-solution (UWS) based selective catalytic reduction (SCR) is currently most promising method to fulfil stringent requirements of upcoming Euro 6 norm on NO_x emissions from diesel engines. Once urea-water-solution spray is injected into hot exhaust gas stream before SCR catalyst, water content evaporates from UWS. Afterwards, ammonia is generated through thermal decomposition of urea and hydrolysis of isocyanic acid. Generated ammonia takes part in various deNO_x reactions as a reductant. The resulting spatial distribution of the reducing agent before the catalyst is a crucial factor for the conversion of NO_x. The uniform distribution and the degree of processing of the reducing agent upstream of the SCR catalyst can be, besides the evaporation and decomposition, also influenced by the spray/wall interaction.

The focus of this paper is therefore the investigation of the spray interaction with both the hot air stream and wall by means of numerical simulation and the validation of mathematical models integrated in commercial CFD code Fire. To predict the generation and distribution of the reducing agent a detailed three-dimensional numerical simulation was performed. UWS droplets were treated with Lagrangian particle tracking, which solves the equation of motion, mass and enthalpy for parcels of droplets with identical properties. Deposition of droplets leads to the formation of a wallfilm which is modelled with a 2D finite volume method in the Fire wallfilm module. To evaluate the influence of varying parameters, well-known spray parameters as an initial condition are essential for a CFD simulation. As modelling of primary breakup is still insufficiently understood, the first step is spray calibration. The single calibration steps of spray were verified with digital CCD (charge-coupled device) camera images, patternator measurements and laser light scattering measurements. After spray calibration the spray/wall-interaction and wallfilm formation were investigated in a rectangular flow channel geometry and obtained simulation results were compared to experimental data.

Key words: gas aftertreatment, selective catalytic reduction, wallfilm, urea water solution, NO_x reduction, computational fluid dynamics

SAŽETAK

Selektivna katalitička redukcija bazirana na vodenoj otopini uree je trenutno najperspektivnija metoda za ispunjavanje strogih zahtjeva nadolazeće Euro 6 norme na NO_x emisije iz diesel motora. Nakon što se vodena otopina uree u obliku spreja ubrizga u struju vrućih dimnih plinova prije katalizatora, dolazi do isparavanja vode iz otopine i stvaranja amonijaka termalnom dekompozicijom uree i hidrolizom izocijanske kiseline. Nastali amonijak sudjeluje u različitim deNOx reakcijama kao reducirajuće sredstvo. Rezultirajuća prostorna raspodjela amonijaka prije katalizatora je ključni faktor učinkovite konverzije NOx-a. Na nju, uz procese isparavanja i dekompozicije, također utječe i interakcija spreja i stijenke.

Stoga je zadatak ovog diplomskog rada istraživanje interakcije spreja s vrućom zračnom strujom i stijenkom uz pomoć numeričke simulacije i validacija matematičkih modela integriranih u komercijalni CFD kod „Fire“. Izvršena je detaljna trodimenzionalna numerička simulacija s ciljem predviđanja nastajanja i raspodjele amonijaka. Kapljice vodene otopine uree su su praćene Lagrangeovim pristupom u kojem se jednadžbe gibanja, očuvanja mase i energije rješavaju za skupine kapljica identičnih svojstava. Deponiranje kapljica dovodi do stvaranja filma na stijenci koji je modeliran dvodimenzionalnom metodom kontrolnih volumena unutar Fire wallfilm modula. U cilju procjene utjecaja različitih parametara potrebna su dobro poznata svojstva spreja kao početni uvjeti za CFD simulaciju. Kako se modeliranje primarnog raspadanja mlaza još uvijek istražuje, prvi korak je kalibracija spreja. Pojedini koraci kalibracije verificirani su snimkama digitalne CCD kamere, mjerenjima s tzv. patternator-om i metodama raspršivanja laserske svjetlosti. Nakon kalibracije spreja istraženi su interakcija spreja i stijenke te formiranje filma na stijenci u geometriji pravokutnog kanala. Dobiveni rezultati uspoređeni su s dostupnim eksperimentalnim podacima.

Ključne riječi: obrada dimnih plinova, selektivna katalitička redukcija, film na stijenci, vodena otopina uree, redukcija dušikovih oksida, računalna dinamika fluida

PROŠIRENI SAŽETAK

Zahtjevi za energijom se stalno povećavaju i nema naznaka da će se taj trend promijeniti u doglednoj budućnosti. Rastuća svjetska populacija zajedno sa sve višim životnim standardom uzrokuje porast potrebne količine energije na globalnoj skali. Većina te energije se još uvijek osigurava izgaranjem fosilnih goriva pri čemu se velike količine zagađujućih tvari ispuštaju u okoliš.

Dozvoljene emisije zagađujućih tvari reguliraju se u razvijenim zemljama preko 30 godina. U bliskoj budućnosti se očekuju nove i sve striktnije regulative. Primjerice, nadolazeća Euro 6 norma postavlja sljedeća ograničenja u pogledu ispuštanja dušikovih oksida (NO_x) iz cestovnih vozila opremljenih diesel motorima s unutarnjim izgaranjem:

- maksimalna dopuštena emisija dušikovih oksida iznosi 80 mg/km, što predstavlja dodatnu redukciju od preko 50 % u odnosu na trenutno vrijedeću Euro 5 normu;
- kombinirane emisije ugljikovodika i dušikovih oksida su ograničene na 170 mg/km.

Strogi zahtjevi Euro 6 norme mogu se zadovoljiti samo kombiniranjem modernih tehnologija u motorima s unutarnjim izgaranjem sa sustavom obrade ispušnih plinova. Za komercijalne dizelske motore to znači korištenje common rail sustava ubrizgavanja goriva s tlakovima ubrizgavanja do 2500 bar, tlakove prednabijanja od 4 bara i recirkulaciju ispušnih plinova do 30 % pri punom opterećenju. Daljnja redukcija emisija može se postići primjenom pogodne metode obrade ispušnih plinova. Trenutno je selektivna katalitička redukcija na bazi vodene otopine uree najperspektivnija metoda za smanjenje emisija dušikovih oksida koje zahtijeva Euro 6 norma.

Otopina uree u vodi u iznosu od 67.5% patentirana je pod trgovačim nazivom AdBlue i služi za generiranje amonijaka kao redukcijskog sredstva. Čisti amonijak nije pogodan za direktno korištenje u vozilima zbog njegovih za okoliš toksičnih svojstava, ali i zapaljivosti te eksplozivnosti u smjesi sa zrakom.

Nakon što se vodena otopina uree u obliku spreja ubrizga u struju vrućih dimnih plinova prije katalizatora, dolazi do isparavanja vode iz otopine i stvaranja amonijaka termalnom dekompozicijom uree i hidrolizom izocijanske kiseline. Nastali amonijak sudjeluje u različitim deNO_x reakcijama kao reducirajuće sredstvo. Rezultirajuća prostorna raspodjela amonijaka prije katalizatora je ključni faktor učinkovite konverzije dušikovih oksida. Na nju, uz procese isparavanja i dekompozicije, također utječe i interakcija spreja i stijenke.

Detaljno razumijevanje složenih fizikalnih i kemijskih procesa koji se odvijaju u sustavima za obradu ispušnih plinova motora s unutrašnjim izgranjem ključno je za njihovo unapređenje kroz konstrukcijski razvoj i optimizaciju. Sveobuhvatno razumijevanje tih procesa i dalje je veliki izazov za istraživače i znanstvenike uslijed njihove kompleksnosti, ali i otežene mogućnosti eksperimentalnog ispitivanja. Naime, intenzivna eksperimentalna ispitivanja u ovakvim sustavima rezultiraju visokim troškovima i dugotrajnim istraživanjima. Ne treba smetnuti s uma ni da ovakva ispitivanja zahtijevaju posebnu pažnju jer se procesi mogu vrlo lako narušiti korištenjem neadekvatne mjerne opreme.

U zadnja dva desetljeća, eksponencijalnim porastom računalne snage, nameće se kao alternativa skupim eksperimentalnim ispitivanjima matematičko modeliranje opisanih procesa uz pomoć Računalne Dinamike Fluida (RDF). Pristup se sastoji u tome da se adekvatnim matematičkim modelom opisuje promatrani fizikalni fenomen, nakon čega se pristupa diskretizaciji interesne domene metodom kontrolnih volumena. Konačno, u posljednjem koraku se jednadžbe modela rješavaju pogodnim numeričkim metodama, nakon čega se dobiveni rezultati prikazuju u grafičkoj formi koja omogućuje njihovu validaciju. Ipak, unatoč navedenim prednostima, u modelima računalne dinamike fluida postoje mnogobrojni izvori pogrešaka, koji unatoč velikim naporima uloženima od strane istraživača i inženjera, još uvijek ne dopuštaju točna kvantitativna predviđanja promatranih fenomena. Računalna dinamika fluida omogućuje skraćivanje vremena i smanjenje troškova razvoja u ranoj, prototipnoj fazi konstruiranja proizvoda. Njome se uz relativno niske troškove već na početku može izvršiti velik broj simulacija kojima se dolazi do kvalitativnog uvida u fiziku promatranog problema, čime se omogućuje odabir svega nekoliko pogodnih prototipova. Oni se zatim izrađuju i detaljno eksperimentalno ispituju kako bi se donio zaključak o optimalnoj konstrukciji proizvoda. Na taj način primjena RDF-a u ranoj fazi razvoja proizvoda značajno skraćuje proizvodni postupak i pridonosi smanjenju troškova razvoja. Međutim, eksperimentalno ispitivanje, ma koliko skupo, još uvijek je neizbježno sredstvo finalizacije razvoja.

U ovom radu je istražena interakcija spreja vodene otopine uree s vrućom zračnom strujom i stijenkom uz pomoć numeričke simulacije te je izvršena validacija matematičkih modela integriranih u komercijalni CFD kod „Fire“.

Prilikom ubrizgavanja vodene otopine uree, sljedeći fizikalni fenomeni zahtijevaju adekvatnu matematičku formulaciju:

- izmjena količine gibanja između kapljica i plinovite faze;

- isparavanje i termoliza kapljica;
- prijenos topline između stijenke i kapljice;
- interakcija spreja i stijenke;
- dvokomponentni film na stijenci uključujući interakciju s plinovitom fazom i stijenkom;
- sekundarno raspadanje spreja.

U navedene fenomene relevantne za opis procesa selektivne katalitičke redukcije trebalo bi ubrojiti i primarno raspadanje mlaza, ali ono je još uvijek u ranoj fazi razvoja pa se nedostatak adekvatnog matematičkog modela nadoknađuje kalibracijom spreja s dostupnim eksperimentalnim podacima. Upravo je to bila prva faza ovog diplomskog rada.

Za glavnu simulaciju bilo je potrebno odrediti inicijalnu brzinu kapljica spreja na izlazu iz mlaznice, nagib rupica u ravnini sapnice, kut spreja te inicijalnu distribuciju veličine kapljica. Snimke propagacije spreja digitalnom CCD kamerom u tesnoj komori poslužile su za određivanje početne brzine kapljica spreja na izlazu iz mlaznice. Iz njih je dobiven dijagram ovisnosti penetracije spreja o vremenu koji je poslužio kao baza za usporedbu s rezultatima simulacije.

Uređaj naziva „patternator“ korišten je za eksperimentalno određivanje tzv. uzorka spreja. Uzorak spreja karakterističan je za pojedinu vrstu sapnice pri danim radnim uvjetima i predstavlja masenu distribuciju spreja na različitim udaljenostima od sapnice. Podešavanjem spomenutog nagiba rupica u ravnini sapnice kao i kuta spreja, moguće je unutar simulacije utjecati na masenu distribuciju spreja i korigirati je dok se ne ostvari zadovoljavajuće poklapanje s eksperimentalnim podacima.

Konačno, posljednji korak kalibracije spreja sastojao se od određivanja početne razdiobe veličine kapljica. Eksperimentalni rezultati dobiveni su na udaljenosti 30 mm od mlaznice uz pomoć metode raspršivanja laserske svjetlosti. Metoda se bazira na principu da kut raspršene laserske svjetlosti ovisi o veličini kapljica. Na taj način je moguće složenim algoritmima odrediti razdiobu veličine kapljica analiziranjem uzorka laserske svjetlosti raspršene na spreju.

Parametri spreja dobiveni opisanom kalibracijskom procedurom služe kao ulazni podaci za glavnu simulaciju gdje se proučava interakcija spreja i stijenke te formiranje filma na stijenci u geometriji pravokutnog kanala dimenzija 970 x 120 x 45 mm.

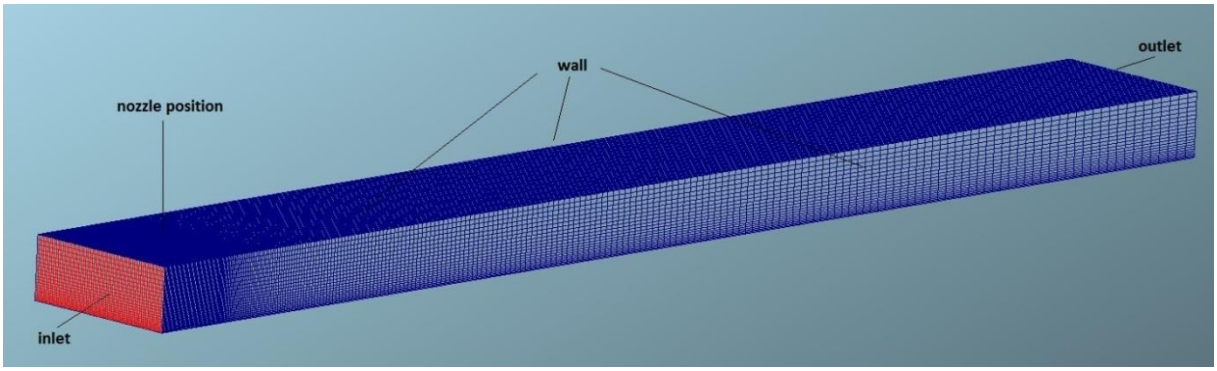

Slika 1. Računalna domena za glavnu simulaciju

Napravljena je analiza za dva slučaja u kojima je variran maseni protok ubrizgane kapljevine (AdBlue-a) i temperatura zraka na ulazu. Simulacijski rezultati pokazuju zadovoljavajuće podudaranje s eksperimentalnim podacima, ali je u eksperimentu nastupila hidroliza izocijanske kiseline koja nije bila modelirana provedenim simulacijama. Na taj način su koncentracije amonijaka bile nešto više od onih koje nastaju čistom termolizom uree.

Nadalje, u eksperimentu je opažen značajan utjecaj površinske napetosti vodene otopine uree na formiranje filma na stijenci. Kako njezin utjecaj nije obuhvaćen trenutnim matematičkim modelom implementiranim u „Fire“, predlaže se njegovo proširenje. Dodatnu komplikaciju za modeliranje predstavljaju depoziti uree i njezinih polimernih produkata na stijenci čiji nastanak i ponašanje u okolini visoke temperature još nije dovoljno istraženo, niti implementirano u komercijalne CFD pakete.

Usprkos navedenim nedostacima, trenutni modeli implementirani u Fire mogu se koristiti s punim povjerenjem kao važan dio modernog inženjerskog razvojnog procesa sa svrhom smanjenja troškova, ali i vremena potrebnog za razvoj modernih sustava selektivne katalitičke redukcije u vozilima. Preporuka za daljnji istraživački rad je poboljšanje simulacija uključivanjem postojećeg modela hidrolize izocijanske kiseline kao i proširenje matematičkih modela unutar „Fire-a“ kako bi uključili efekte površinske napetosti i nastanak ureinih depozita u okolini karakterističnoj za ispušne sustave diesel motora.

1. INTRODUCTION

Energy demands are rapidly increasing and it is going to be so in foreseeable future. Growing world population together with higher life standard causes increase of the required amount of energy on a global scale. The major part of that amount is still supplied by fossil fuels whose usage in combustion systems releases large quantities of pollutants into the environment. Since fossil fuels are not renewable energy resources, its rationale usage is obligate.

Allowable pollutant emissions from combustion sources have been regulated in developed countries for over 30 years. New and stringent regulations are expected in foreseeable future. For example, the new Euro 6 standard will come into force on 1 September 2014 and here are some requirements to illustrate its strictness [1]:

- NO_x emissions from cars and vehicles intended to be used for transport will be restricted at 80 mg/km, which is an additional reduction of more than 50 % compared to the currently valid Euro 5 standard;
- combined emissions of hydrocarbons and nitrogen oxides of above mentioned vehicles will be reduced to 170 mg/km.

The consequence of more stringent regulations and non-renewability of currently most used fossil fuels for supplying world energy demands is a request for increased energy efficiency as well as for reduction of pollutant emissions, especially NO_x.

Strict requirements of upcoming Euro 6 norm can only be met by a combination of new exhaust gas aftertreatment and engine technologies. For commercial diesel engines this means the use of common rail fuel injection systems with pressures of up to 2500 bar, charging pressures of 4 bar and exhaust gas recirculation up to 30 % at full load [2]. Further reduction of the NO_x emissions below the emission limits can be achieved by suitable exhaust gas aftertreatment system. The most promising technology for the reduction of NO_x in the exhaust is the selective catalytic reduction (SCR) with ammonia, which is produced from precursor substances like urea in the exhaust gas system. Due to combustion with oxygen excess in diesel engines, O_2 is present in larger amounts in the exhaust gas, which makes a simple reduction of NO_x very difficult. Generally, all applicable reducing agents prefer to react with oxygen prior to the conversion of the less reactive NO, due to higher activation energy of reaction with NO. Application of a catalyst lowers that energy, so that this reaction proceeds

selectively towards nitrogen without reductant being oxidized. Hence the generally known name - selective catalytic reduction (SCR).

Urea-water solution (UWS) is most commonly used ammonia precursor for mobile SCR applications since it represents no danger for environment in case of a traffic accident. AdBlue is commercial name for an aqueous urea solution blended with 32.5% high purity urea and 67.5% deionized water.

Once urea-water-solution spray is injected into hot exhaust gas stream before SCR catalyst, water content evaporates from UWS. Afterwards, ammonia is generated through thermal decomposition of urea and hydrolysis of isocyanic acid:

$$(NH_2)_2CO \rightarrow NH_3 + HNCO \quad \textbf{(1)}$$

Hydrolysis of isocyanic acid:

$$HNCO + H_2O \rightarrow NH_3 + CO_2 \quad \textbf{(2)}$$

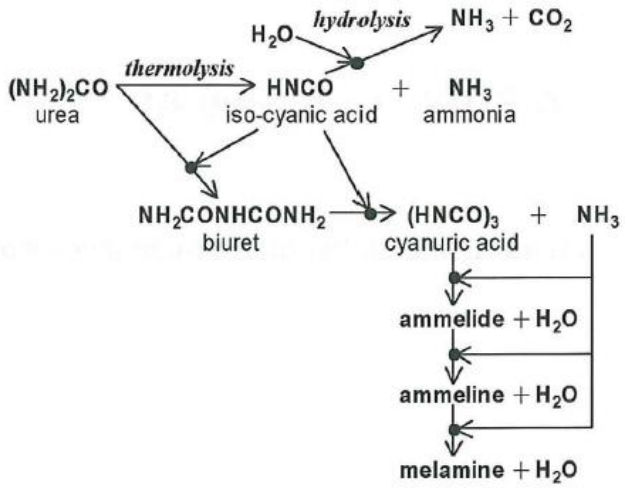

Figure 1. Reaction scheme of urea [3]

Generated ammonia takes part in various deNO_x reactions as a reductant (among other things)[4]:

Desirable reduction:

$$4NH_3 + 4NO + O_2 \rightarrow 4N_2 + 6H_2O \text{ (standard SCR)} \quad \textbf{(3)}$$

$$4NH_3 + 6NO \rightarrow 5N_2 + 6H_2O \quad \textbf{(4)}$$

$$8NH_3 + 6NO_2 \rightarrow 7N_2 + 12H_2O \quad \textbf{(5)}$$

$$4NH_3 + 2NO_2 + 2NO \rightarrow 4N_2 + 6H_2O \text{ (fast SCR)} \quad \textbf{(6)}$$

$$4HNCO + 6NO \rightarrow 5N_2 + 2H_2O + 4CO_2 \quad \textbf{(7)}$$

Direct urea reduction:

$$2(NH_2)_2CO + 6NO \rightarrow 5N_2 + 2CO_2 + 4H_2O \quad \textbf{(8)}$$

Undesirable reaction/oxidation:

$$2NH_3 + 8NO \rightarrow 5N_2O + 3H_2O \quad \textbf{(9)}$$

$$4NH_3 + 4NO + 3O_2 \rightarrow 4N_2O + 6H_2O \quad \textbf{(10)}$$

$$4NH_3 + 5O_2 \rightarrow 4NO + 6H_2O \quad \textbf{(11)}$$

$$4NH_3 + 7O_2 \rightarrow 4NO_2 + 6H_2O \quad \textbf{(12)}$$

$$4NH_3 + 4O_2 \rightarrow 2N_2O + 6H_2O \quad \textbf{(13)}$$

$$4NH_3 + 3O_2 \rightarrow 2N_2 + 6H_2O \quad \textbf{(14)}$$

Undesirable degradation:

$$NH_3 + SO_2 + \frac{1}{2}O_2 + H_2O \rightarrow NH_4(HSO_4) \quad \textbf{(15)}$$

$$2NH_3 + SO_2 + \frac{1}{2}O_2 + H_2O \rightarrow (NH_4)_2SO_4 \quad \textbf{(16)}$$

$$(NH_2)_2CO \rightarrow \text{polymeric products} \quad \textbf{(17)}$$

$$2NH_3 + 2NO_2 \rightarrow NH_4NO_3 + N_2 + H_2O \quad \textbf{(18)}$$

$$HNCO + 3NH_3 \rightarrow \text{melamine } (C_3N_6H_6)_x \quad \textbf{(19)}$$

NO_x in diesel exhaust is usually composed of >90 % NO and only 5-10 % of NO_2. Therefore, the main reaction of SCR with ammonia is reaction (3). The reaction consuming no oxygen (4) is much slower and is therefore not relevant in combustion engines exhaust gas aftertreatment. The reaction rate with equimolar amounts of NO and NO_2 (6) is much faster than the main reaction and therefore is called fast SCR reaction. The NO_2 needed for fast SCR reaction might be produced from engine emitted NO in a pre-oxidation catalyst.

Under ideal spraying conditions for the urea solution, engine test results have shown a stoichiometric ratio 2.2.-2.9 mol of NO per 1 mol of urea consumption [4]. This is equal to a weight ratio 0.67-0.9 g of urea required to reduce 1 g of NO in the exhaust. So, it can be concluded that standard and fast SCR reaction are backed up by reactions (7) and (8).

Considering undesirable reactions, the reaction of NH_3 with oxygen or NO should be minimized because they not only consume reducing agent but also generate more unwanted

NO_x species. Formation of melamine and polymeric products could be one major loss of urea responsible for non-stoichiometric balance of urea consumption and could lead to degradation of catalyst surface.

1.1. Challenges for the mobile UWS based SCR

The major goal of urea-SCR in mobile applications is the reduction of the required catalyst volume while still maintaining a high selectivity for the SCR reaction over a wide temperature range. The much shorter residence time of the exhaust gas in the catalyst leads to higher secondary emissions of ammonia and isocyanic acid originating from the reducing agent. In mobile diesel engine load and engine speed vary often and abruptly, which causes permanent changes of flow and temperature of the exhaust gas. Therefore, a sophisticated control for the dosage of the reducing agent is mandatory.

Confined space for catalyst installation in vehicles is a problem furthermore aggravated by two unfavourable features of the diesel engine: wide range of exhaust gas temperatures and larger exhaust flow rate compared to Otto process. Therefore, the volumetric activity of the catalyst must be improved and this may be realized by the following means:

- increase of the intrinsic activity of the SCR catalyst;
- increase of the cell density of the SCR;
- increase of the NO2 fraction in the exhaust by passing the gas over oxidation catalyst in order to make use of reaction (6).

Aiming at compact $DeNO_x$ systems leads to short residence time ahead of the SCR catalyst which causes significant problem for mixing of NO_x and reducing agent. Ammonia slip from the catalyst is further problem in mobile SCR applications because of it's well known toxicity. Because exhaust gas temperatures vary between 100°C and 650°C, the catalyst temperature will vary correspondingly and this leads to varying amounts of ammonia adsorbed on the catalyst. If this ammonia isn't taken into consideration by the dosing system, excess of ammonia will slip through catalyst into environment. The following measures can minimize ammonia slip from mobile SCR system:

- use of coated instead of extruded catalysts (less active mass per catalyst volume);
- use of optimized dosing strategy – catalyst activity determined mainly by its actual temperature should be taken into account;
- additional oxidation catalyst could be added downstream of the SCR catalyst.

Other difficulties related to the use of urea, such as: emission of isocyanic acid, the high freezing point of aqueous urea solution, possible formation of high molecular weight products and long term stability of SCR catalysts, are described in detail in [5] and [6].

1.2. Work outline

The spatial distribution of the reducing agent before the SCR catalyst is a crucial factor for the conversion of NO_x. The uniform distribution and the degree of processing of the reducing agent upstream of the SCR catalyst can be, besides the evaporation and decomposition, also influenced by the spray/wall interaction.

The focus of this thesis is therefore the investigation of the spray interaction with both the hot air stream and wall by means of numerical simulation and the validation of mathematical models integrated in commercial CFD code Fire. To predict the generation and distribution of the reducing agent a detailed three-dimensional numerical simulation was performed. UWS droplets were treated with Lagrangian particle tracking, which solves the equations of motion, mass and enthalpy for parcels of droplets with identical properties. Deposition of droplets leads to the formation of a wallfilm which is modeled with a 2D finite volume method in the Fire wallfilm module. To evaluate the influence of varying parameters, well-known spray parameters as an initial condition are essential for a CFD simulation. As modelling of primary breakup is still insufficiently understood, the first step is spray calibration. The single calibration steps of spray were verified with digital CCD (charge-coupled device) camera images, patternator measurements and laser light scattering measurements. After spray calibration the spray/wall-interaction and wallfilm formation were investigated in a rectangular flow channel geometry and obtained simulation results were compared to experimental data.

Well established mathematical models of all relevant physical phenomena regarding SCR that are implemented in commercial CFD codes form basis for design of modern selective catalytic reduction systems including dozing apparatus [7][8][9].

2. MATHEMATICAL MODELS

In order to include all relevant phenomena appearing during injection of urea-water solution into confined space of mobile SCR systems we need suitable mathematical description of the following processes:

- momentum interaction between gas phase and droplets;
- evaporation and thermolysis of droplets;
- heat transfer between wall and droplets;
- spray/wall interaction;
- two-component wall film including interaction with gas phase and exhaust tube;
- secondary break-up of spray.

This section presents basics of mathematical models implemented in commercial CFD code Fire used for conducting of numerical simulations.

2.1. Fundamentals of fluid mechanics

Fluid mechanics is theoretical and experimental science which deals with fluid motion problems. Analytical solution methods are basis for the theoretical approach whose solutions give a complete insight into the fundamental physics of the observed phenomena and also provide the possibility for complete parameter analysis in the mathematical model. Unfortunately, most of the fluid problems are described with nonlinear partial differential equations which don't have general analytical solution. This is the main reason why experimental approach was dominant in the past. The main drawback of this approach is limited quantity of provided information about fluid flow problem, which is directly dependent upon the number of sensors mounted on the experimental setup. Exponential increase in computing power has laid down foundations for numerical solving of mathematical models describing fluid motion. This marked the beginning of the development of the third branch of fluid mechanics – computational fluid dynamics.

Computational fluid dynamics (CFD) is relatively new branch of fluid mechanics which deals with fluid motion and heat and mass transfer problems via numerical simulations performed on computer. CFD has a broad area of application in engineering. Some of the well-known applications of CFD are listed below:

- vehicle aerodynamics;
- hydrodynamics;
- power plants (combustion engines, gas turbines, boilers, etc.);
- turbomachinery (flow inside rotating parts);
- chemical engineering (polymer molding, mixing and separation processes, etc.);
- civil engineering (HVAC systems);
- hydrology and oceanography (rivers, oceans, estuaries, etc.);
- meteorology (weather forecasting);
- biomedical engineering (blood flow through arteries and veins).

Advantages of computational fluid dynamics in comparison with experimental approach are as follows:

- significant decrease in development time and costs;
- ability to simulate large systems;
- possibility of simulating under hazardous conditions and overloading;
- decrease of energy consumption;
- complete and detailed representation of fluid flow problem.

Some of the CFD drawbacks:

- in some cases can be more expensive than experimental approach (e.g. for determination of pump characteristics);
- restriction on problems that can be described with reliable mathematical models.

Each simulation begins with the definition of the problem and the selection of a mathematical model. The mathematical model is usually presented with a system of partial differential equations integrated over the control volume. Any such system of equations has the general solution and particular solution which is characterized by initial and boundary conditions that unambiguously define observed problem. Commercial CFD codes, such as AVL Fire, have built-in mathematical model and user can via graphical interface choose desired variant of the model that fits his problem.

The second step of numerical simulation is to solve selected mathematical model by the means of numerical methods. Numerical solving procedure consists of three steps. In the first step domain is discretized with finite volumes. The result of spatial discretization is called geometric mesh. Then, on the defined geometrical mesh, equations of the mathematical model are discretized. The result of discretization is a system of algebraic equations that can be

linear or nonlinear depending on the nature of associated partial differential equations. Nonlinear algebraic equations are solved by the means of iterative solver.

The final step of CFD numerical simulation is called post processing and includes graphical representation of numerical results such as scalar, vector and tensor fields, heat and mass fluxes, forces, etc.

Organization scheme of commercial CFD codes follows the chronological sequence of CFD simulation mentioned above. It consists of: preprocessor which is utilized for geometric mesh generation and definition of boundary and initial conditions, processor which solves defined mathematical models by the means of numerical based algorithms and postprocessor which is used for visualization and treatment of the CFD simulation results.

2.1.1. Governing equations of fluid flow and heat transfer

The governing equations of fluid flow represent mathematical statements of the conservation laws of physics [10]:

- the mass of fluid is conserved;
- the rate of change of momentum equals the sum of the forces on a fluid particle (Newton's second law);
- the rate of change of energy is equal to the sum of the rate of heat addition to and the rate of work done on a fluid particle (first law of thermodynamics).

The fluid is regarded as a continuum, which means that the molecular structure of matter and molecular motions may be ignored and that the behaviour of the fluid is described in terms of macroscopic properties, such as velocity, pressure, density, temperature, etc.

Here presented equations are developed for collection of fluid elements which make up a region fixed in space, i.e. control volume (Eulerian approach). Fluid is regarded as Newtonian and compressible, which means that it can be described with following set of equations in conservative form:

Continuity equation

$$\frac{\partial \rho}{\partial t} + \operatorname{div}\left(\rho \boldsymbol{u}\right) = 0 \qquad \textbf{(20)}$$

x-momentum equation

$$\frac{\partial (\rho u)}{\partial t} + \operatorname{div}\left(\rho u \boldsymbol{u}\right) = -\frac{\partial p}{\partial x} + \operatorname{div}\left(\mu \operatorname{grad} u\right) + S_{Mx} \qquad \textbf{(21)}$$

y-momentum equation

$$\frac{\partial(\rho v)}{\partial t}+\operatorname{div}\left(\rho v\boldsymbol{u}\right)=-\frac{\partial p}{\partial y}+\operatorname{div}\left(\mu\operatorname{grad}v\right)+S_{My} \tag{22}$$

z-momentum equation

$$\frac{\partial(\rho w)}{\partial t}+\operatorname{div}\left(\rho w\boldsymbol{u}\right)=-\frac{\partial p}{\partial z}+\operatorname{div}\left(\mu\operatorname{grad}w\right)+S_{Mz} \tag{23}$$

Energy equation

$$\frac{\partial(\rho i)}{\partial t}+\operatorname{div}\left(\rho i\boldsymbol{u}\right)=-p\operatorname{div}\boldsymbol{u}+\operatorname{div}\left(k\operatorname{grad}T\right)+\Phi+S_i \tag{24}$$

Equations of state

$$p=p\left(\rho,T\right)\text{ and }i=i(\rho,T) \tag{25}$$

This system of equations is mathematically closed because it contains equal number of equations and unknown functions, namely seven. It can be solved provided that suitable initial and boundary conditions are supplied.

Significant commonalities between presented governing equations justify introduction of a general variable ϕ, which enables us to write general conservative form of all fluid flow equations, called the transport equation:

$$\frac{\partial(\rho\phi)}{\partial t}+\operatorname{div}\left(\rho\phi\boldsymbol{u}\right)=\operatorname{div}\left(\Gamma\operatorname{grad}\phi\right)+S_\phi \tag{26}$$

In words, rate of increase of ϕ of fluid element plus net rate of flow of ϕ out of fluid element equals to sum of rate of increase of ϕ due to diffusion and rate of increase of ϕ due to sources. Equation (26) is used as a starting point for computational procedures in the finite volume method [10][11][12]. The key step of the finite volume method is the integration of (26) over a three-dimensional control volume (CV):

$$\int_{CV}\frac{\partial(\rho\phi)}{\partial t}\mathrm{d}V+\int_{CV}\operatorname{div}\left(\rho\phi\boldsymbol{u}\right)\mathrm{d}V=\int_{CV}\operatorname{div}\left(\Gamma\operatorname{grad}\phi\right)\mathrm{d}V+\int_{CV}S_\phi\mathrm{d}V \tag{27}$$

2.2. Liquid spray

2.2.1. Fundamentals

Liquid sprays are irreplaceable tool for introduction of liquid phase into gaseous one and therefore are used in a wide variety of technical fields such as: process industry, pharmaceutical industry, agriculture, industrial boilers, internal combustion engines, gas turbines, rockets, spray painting, spray cooling, fire extinction, etc.

This work deals with sprays produced by the low pressure atomization technique that are utilized in the exhaust gas aftertreatment and here presented basics regard high pressure sprays. The liquid enters the pre-catalyst chamber at high velocity in the form of a liquid jet and then disintegrates, first into fragments and later into small droplets.

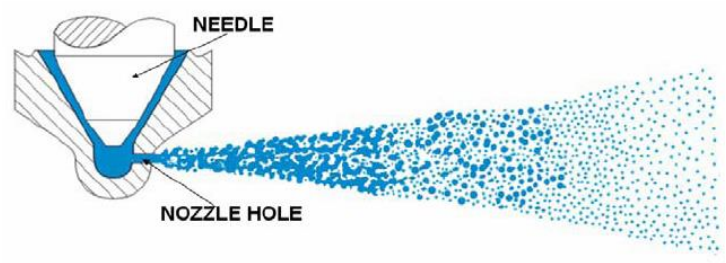

Figure 2. Representation of liquid spray [13]

The break-up processes of the injected liquid spray can be generally classified as:

- primary break-up of the liquid jet - break-up of the liquid jet into fragments and further disintegration of fragments into spherical droplets;
- secondary break-up of the liquid jet - spherical droplets from primary break-up further disintegrate into smaller droplets and fragments by means of aerodynamic forces.

There is no sharp boundary between primary and secondary break-up regions, as is illustrated on Figure 3. On the same Figure can also be seen that primary break-up happens near the nozzle exit, while secondary break-up happens far from the nozzle.

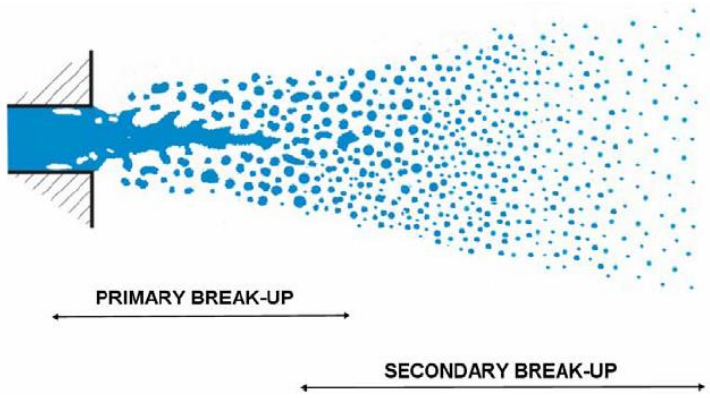

Figure 3. Representation of break-up processes [13]

Kelvin-Helmholtz and Rayleigh-Taylor hydrodynamic instabilities on the liquid gas interface cause break-up processes by producing waves on the liquid surface [17]. Kelvin-Helmholtz instabilities are caused by viscous forces due to relative motion between liquid and surrounding gas phase, while Rayleigh-Taylor instabilities happen on droplet due to inertia of

decelerated droplet. The liquid jet break-up process is characterized by Reynolds number, Weber number and Ohnesorge number. The Reynolds number represents ratio of inertial and viscous forces and is used for characterization of the fluid flow. The Reynolds number is mathematically defined as:

$$Re = \frac{\rho d v}{\mu} \tag{28}$$

where d is nozzle exit diameter, v is relative velocity of droplets, ρ is density of a liquid and μ is dynamic viscosity of a liquid.

The Weber number is the most important parameter used to describe the rate of break-up. It relates forces on droplet from dynamic pressure and surface tension forces. It is defined as:

$$We = \frac{\rho d v^2}{\sigma} \tag{29}$$

where σ is a surface tension at the liquid-gas interface.

The Ohnesorge number is the ratio of the viscous and inertial and surface tension forces. It can be derived using Reynolds and Weber number:

$$Oh = \frac{\sqrt{We}}{Re} \tag{30}$$

Four different primary break-up regimes can be identified using three non-dimensional numbers mentioned above: Rayleigh break-up regime, first wind-induced regime, second wind-induced regime and atomization regime [13]. Only last regime is relevant four our study since we are going to simulate UWS injection system. In that case, cavitation and turbulence that are generated inside the nozzle are main break-up mechanisms for primary break-up. Since the secondary-break up happens far away from nozzle, aerodynamic forces play important role as a main break-up mechanism. The Weber number determines secondary break-up type.

Spray behaviour is influenced by different spray regimes which are illustrated on Figure 4. The zone of primary break-up is also termed as dense spray and the zone of secondary break-up is termed as thin and dilute spray. Dense spray region is located near the nozzle exit and is characterized by negligible fraction of gas phase. Thin spray regime occurs downstream from the dense spray and here is mass fraction of liquid phase still significant in contrast to its volume fraction. The last region of dilute spray is located far from the nozzle and consists of fully atomized liquid.

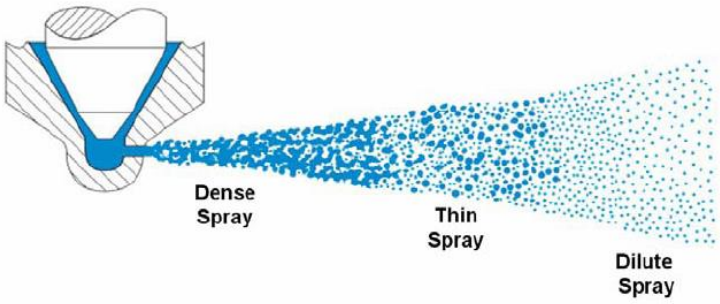

Figure 4. Representation of spray regimes [13]

Nozzle design, injected liquid properties and operating conditions define main liquid spray characteristics: the droplet size distribution, the spray cone angle, the shape of spray pattern and the spray penetration.

The droplet size distribution describes the quality of atomization which is prerequisite for efficient combustion process. Characteristics of high level of atomization are small mean droplet diameter and narrow droplet diameter distribution curve, i.e. small deviations from mean droplet diameter.

Geometric characteristics - spray penetration and spray angle are illustrated on the figure below.

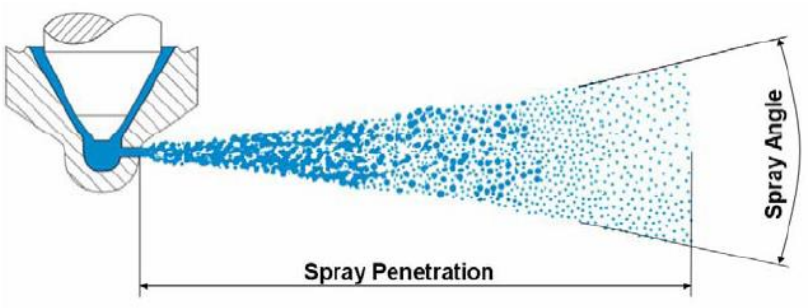

Figure 5. Representation of spray characteristics [13]

2.2.2. Spray modelling – basic equations

Experimental observations as well as the knowledge obtained from the instability analyses form the basis for numerical modelling of liquid spray.

The most commonly used method for spray calculation today is Discrete Droplet Method (DDM) [17]. Taking into account current state of CFD techniques, it would be practically impossible to solve differential equations for the trajectory, momentum, heat and mass transfer of every single spray droplet. DDM simplifies spray modelling by introducing

parcels which are groups of identical non-interacting droplets. Thus, one member of the group, i.e. droplet of certain size, represents the behaviour of the complete parcel. That way, only differential equations of parcels are numerically solved which significantly reduces computation time and required computing power.

Droplet parcels are introduced in the flow domain with initial conditions of position, size, velocity, temperature and number of particles inside the parcel. Lagrangian description of motion is then used for tracking the parcels through the computational grid. A drawback of the standard DDM is the treatment of Lagrangian parcels as point sources for physical quantities for the Eulerian gas flow field.

From the Newton's second law of motion which states that the net force on an object is equal to the rate of change of its linear momentum in an inertial reference frame follows droplet momentum equation:

$$m_d \frac{du_{id}}{dt} = F_{idr} + F_{ig} + F_{ip} + F_{ib} \quad \textbf{(31)}$$

where m_d and u_{id} are droplet mass and droplet velocity respectively, F_{idr} is the drag force, F_{ig} is a force including the effects of gravity and buoyancy, F_{ip} is the pressure force and F_{ib} summarizes other external forces. Comparing the magnitude of all forces, the drag force is only relevant force for fuel spray injection application. Therefore follows:

$$m_d \frac{du_{id}}{dt} = F_{idr} \quad \textbf{(32)}$$

After integrating above equation, u_{id} could be obtained and from this we can solve differential equation for the trajectory:

$$\frac{dx_{id}}{dt} = du_{id} \quad \textbf{(33)}$$

In commercial CFD code Fire turbulent dispersion, evaporation of droplets, the droplet-gas momentum exchange, secondary break-up, droplet collision and droplet-wall interaction are covered with set of models that are summarized in [14].

2.2.3. Spray evaporation

The mathematical model used to perform the calculation of the evaporation processes is Abramzon/Sirignano [15]. This model represents the extension of classical droplet vaporization model [16] and includes important effects such as variable physical properties, non-unitary Lewis number in the gas phase and influence of Stefan flow on the heat and mass

transfer. It requires a relatively small amount of computational time per droplet and therefore, it is suitable for spray calculations which simultaneously trace many individual droplets.

This approach relies on the classic film theory where the resistance to heat and mass transfer are modelled by fictional gas films of constant thickness: δ_T and δ_m. However, in the case of an evaporating droplet these values have to be corrected by the factors F_T and F_M representing the relative change of film thicknesses due to Stefan law. Droplet evaporation is described by the empirical Nusselt and Sherwood numbers derived from experiments using single droplets:

$$\dot{m} = \pi \bar{\rho}_g \bar{\beta}_g D_d Sh^* \ln(1+B_Y) \tag{34}$$

$$\dot{m} = \pi \frac{\bar{k}_g}{\bar{c}_{pF}} D_d Nu^* \ln(1+B_T) \tag{35}$$

where D_d is the droplet diameter, and $\bar{\rho}_g$, $\bar{\beta}_g$, $\bar{k}_g$ are the density, binary diffusion coefficient and thermal conductivity of the gas mixture at reference conditions, $\bar{c}_{pF}$ is the specific heat capacity of the vapour and B_Y and B_T are mass and heat transfer numbers, also called Spalding numbers. The mass transfer number is given as

$$B_Y = \frac{Y_{VS} - Y_{V\infty}}{1 - Y_{VS}} \tag{36}$$

where Y_V is the vapour mass fraction and index S denotes the condition at droplet surface, while index ∞ denotes the ambient condition. Physical properties in (34) and (35) are evaluated at reference temperature and reference vapour concentrations using the 1/3 rule recommended by [17]:

$$\bar{T} = T_S + \frac{1}{3}(T_\infty - T_S) \tag{37}$$

$$\bar{Y}_S = Y_{V,S} + \frac{1}{3}(Y_{V,\infty} - Y_{V,S}) \tag{38}$$

The non-dimensional heat and mass transfer coefficients *Nu** and *Sh** are modified Nusselt and Sherwood numbers, which are given as follows:

$$Nu^* = 2 + \frac{(Nu_0 - 2)}{F_T} \tag{39}$$

$$Sh^* = 2 + \frac{(Sh_0 - 2)}{F_M} \tag{40}$$

where Nu_0 and Sh_0 are Nusselt and Sherwood number of the non-evaporating droplet:

$$Nu_0 = 2 + 0.552 Re^{1/2} Pr^{1/3} \quad \textbf{(41)}$$

$$Sh_0 = 2 + 0.552 Re^{1/2} Sc^{1/3} \quad \textbf{(42)}$$

The diffusional film correction factors F_M and F_T represent the relative change of film thicknesses due to Stefan flow. *F(B)* is the universal function for both factors:

$$F(B) = (1+B)^{0.7} \frac{\ln(1+B)}{B} \quad \textbf{(43)}$$

Finally, the algorithm for calculation of heat and mass transfer is [14]:

1. Evaluate Y_{VS} at the droplet surface.
2. Calculate average physical properties in the gas film using the reference temperature and fuel concentration.
3. Calculate Nusselt and Sherwood number for a non-evaporating droplet, Nu_0 and Sh_0.
4. Get B_Y, F_M, Sh^*.
5. Calculate the mass evaporation rate according to (34).
6. Assume the value of B_T using a value from the previous time step or iteration.
7. Calculate the modified Nusselt number Nu^* and correct the heat transfer number B_T by comparing (34) and (35).

$$B_T = (1+B_Y)^{\phi} - 1 \quad \textbf{(44)}$$

where ϕ is

$$\phi = \frac{\bar{c}_{pF}}{\bar{c}_{pG}} \frac{Sh^*}{Nu^*} \frac{1}{Le} \quad \textbf{(45)}$$

8. If the difference between assumed and the corrected value of B_T is too large, go back to step 6.
9. Calculate the heat transferred into droplet:

$$Q_s = \dot{m} \left(\frac{\bar{c}_{pF}(T_\infty - T_S)}{\bar{B}_T} - L(T_S) \right) \quad \textbf{(46)}$$

2.2.4. Secondary break-up model

As mentioned before, in secondary break-up spherical droplets from primary break-up further disintegrate into smaller droplets and fragments by means of aerodynamic forces. Although Fire contains several secondary break-up models, here will be presented basics of TAB model, which was used for conducting spray simulations.

In TAB model break-up is modelled by the analogy between an oscillating droplet and a spring mass system. The external force is assumed to be analogous to the gas aerodynamic force, the spring force analogous to the surface tension and the damping forces analogous to the liquid viscosity [14].

$$\ddot{y} = \frac{C_F}{C_b}\frac{\rho_g}{\rho_l}\frac{u^2}{r^2} - \frac{C_k\sigma}{\rho_l r^3}y - \frac{C_d\mu_l}{\rho_l r^2}\dot{y}, \qquad \textbf{(47)}$$

y is the dimensionless displacement of the equator of the droplet from its equilibrium position, ρ_g and ρ_l are the gas and liquid densities, u is the relative velocity between the gas and the droplet, r is the droplet radius, σ the gas-liquid surface tension, μ_l the liquid viscosity, and C_F, C_k, C_d and C_b are dimensionless constants determined by mathematical analysis and experiments.

If y>1 the parent droplet breaks up and smaller product droplets are created. Their normal velocity is equal to the normal oscillating velocity of the parent drop at the just before the break-up. This way the spray angle of the jet is calculated by the means of the model itself and does not need to be defined before calculation.

2.2.5. Evaporation and thermolysis of UWS droplets

Despite numerous experimental studies [18][19][20] theoretical understanding of evaporation and decomposition of UWS droplets is still far from satisfactory. Theoretical study conducted by Birkhold et al. [21] is implemented in Fire and represents optimum between results accuracy and computational demands. At elevated temperatures the evaporation of liquid starts. Since water has a lower boiling point then urea, the vapour which evaporates first consist mainly of water. Whether is urea vapour also produced is questionable, since urea is known to decompose directly via thermolysis from solid or liquid. This approach assumes two stage process – pure water evaporation until the drop is composed of urea only and subsequent thermolysis. It is assumed that droplets remain spherical

throughout the evaporation and decomposition processes, as well as that no crystallization of urea occurs.

2.2.5.1. Water evaporation

In order to evaluate the influence of solved urea on the evaporation of water, Rapid Mixing model is employed. Within this model infinite high transport coefficients are assumed for the liquid phase, resulting in spatial uniform temperature, concentration and fluid properties in the droplet, but those quantities will change in time [15]. The variation of urea concentration of the droplet can be evaluated by:

$$\frac{dY_u}{dt} = -\frac{\dot{m}_{vap}}{m_d} Y_u \qquad \textbf{(48)}$$

It should be noted that mass flow from liquid to gaseous phase is defined to be negative. Evaporation rates are calculated using the previously mentioned Abramzon-Sirignano model (see section 2.2.3.).

2.2.5.2. Urea thermolysis

Urea melts at 406 K and the thermal decomposition of urea into ammonia and isocyanic acid starts. It is generally accepted that two different ways for the thermal decomposition can be derived:

- evaporation of molten/solid urea to gaseous urea, which decomposes in gas phase into NH_3 and HNCO;
- direct thermolysis from molten/solid urea to gaseous NH_3 and HNCO as shown in Figure 6.

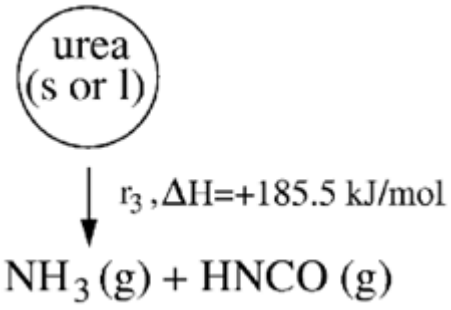

Figure 6. Direct thermolysis from solid/molten urea [21]

This model assumes the latter option and since there is no phase change of urea, an alternative way as used for the evaporation of water must be taken to calculate the urea decomposition rate. For this purpose Arrhenius-type expression is used:

$$\frac{dm_u}{dt} = -\pi D_d A e^{(-E_a/RT_d)} \quad \textbf{(49)}$$

where A is a frequency rate and E_a is activation energy. Experimental data from Yim et al. [22] were used for a default parameter fit.

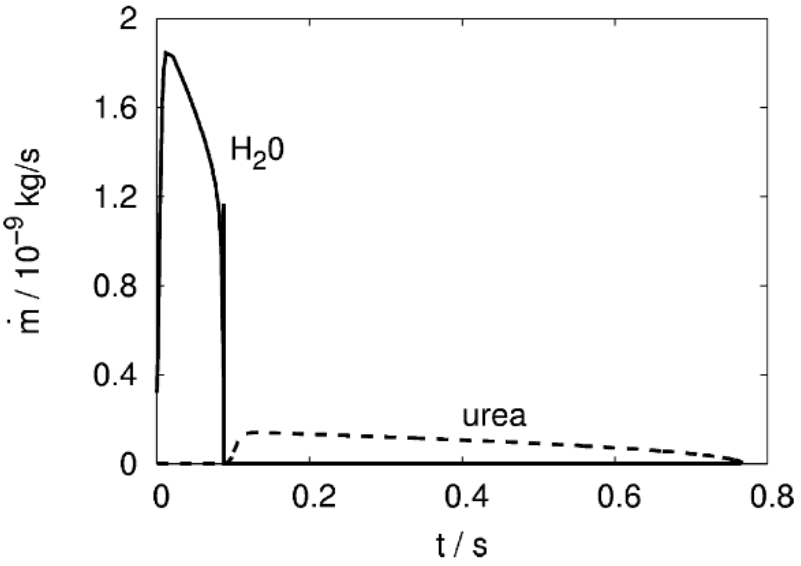

Figure 7. Mass flow of water and urea during evaporation and decomposition [21]

Figure 7. shows calculated mass fluxes of water vapour and urea due to evaporation and decomposition for specific case. However, generalized qualitative analysis could be given because trends remain the same regardless of the observed case.

The evaporation mass flow increases as the droplet heats up and decreases as the droplet diameter decreases. The decomposition of urea occurs at lower rates than the evaporation of water. This is a combination of the higher particle temperature, and thus a lower heat transfer and the higher reaction enthalpy of urea.

Wallfilm approach for evaporation of UWS is similar, except thermolysis occurs when mass fraction of water is less than 5 %.

2.3. Wallfilm

2.3.1. Fundamentals

Fuel deposition in the inlet manifold due to incomplete evaporation and wall collisions of injected droplets is negative phenomenon whose occurrence causes a reduction of potential engine performance and an increase in pollutant emissions [14]. The film's velocity is just a few percentage of mean air stream's velocity due to great difference in air and fuel viscosities. Consequently, this leads to an undesired storage of fuel liquid phase on the manifold walls. Experimental investigation of wallfilm formation phenomena can't be performed in intake manifolds of practical combustion engines without disruption of engine's operational parameters. Therefore, numerical simulation is utilized.

Evaporation of fuel and spray-wall interactions are the most important physical mechanisms that lead to the formation of wall film. Since fuel evaporation is today relatively well understood, we will put our focus on the available knowledge of physics behind spray-wall interactions.

There are four different regimes of spray-wall interactions depending on a dimensionless wall temperature and a dimensionless droplet velocity [23]. Dimensionless temperature is defined as follows:

$$T^* = \frac{T_W}{T_S} \tag{50}$$

where T_W is wall temperature and T_S is droplet saturation temperature.

Dimensionless droplet velocity is defined as:

$$K = \frac{(\rho_d d_d)^{3/4} u_{d,\perp}^{5/4}}{\sigma_d^{1/2} \mu_d^{1/4}} \tag{51}$$

where ρ_d is the density of droplet, d_d is droplet diameter, $u_{d,\perp}$ is the wall normal component of the droplet velocity, σ_d is a surface tension on the droplet-gas interface and $\mu_d^{1/4}$ is the dynamic viscosity of a droplet.

Deposition:

- occurs at low droplet velocities and if $T^*<1.1$;
- impacting droplets are completely deposed on the wall and create wallfilm.

Splash:

- occurs at higher droplet velocities and if $T^*<1.1$;

- particles are atomized and smaller secondary droplets are formed after the impact;
- a fraction of the droplet mass is transferred to the wallfilm.

Rebound:

- occurs at low impact velocities and if $T^*>1.1$;
- vapour layer between droplet and wall is formed that prevents a direct contact of the droplet with the wall and leads to a reflection of impinging droplet (the Leidenfrost effect);
- there is no wallfilm formed.

Thermal breakup:

- occurs at higher impact velocities and if $T^*>1.1$;
- the droplet disintegrates into secondary drops;
- there is no wallfilm formed.

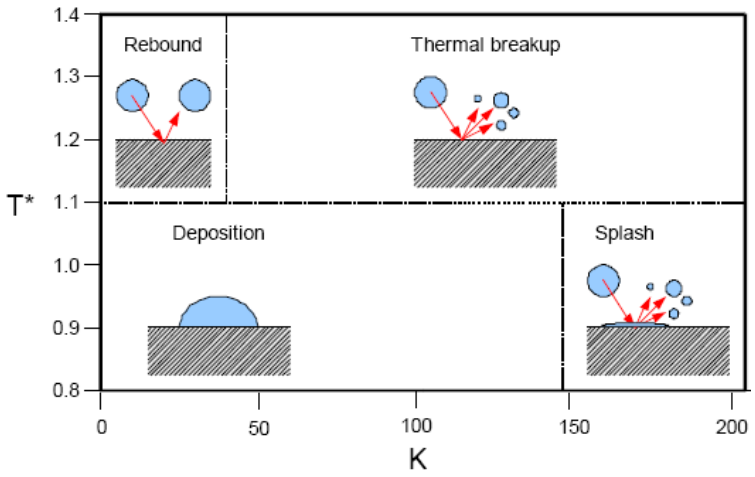

Figure 8. Spray-wall interaction diagram [14]

2.3.2. Wallfilm modelling

Fundamental assumptions and simplifications of the wallfilm model are listed below:

- gas and wallfilm flow are treated as separate single phases; the coupling of the two phases is achieved by a modified set of boundary conditions based on semi-empirical relations;
- the film thickness is very small in relation to the mean diameter of the gas flow, so no adaptation of the volume grid to the film surface is necessary;

- due to thin film and its small velocity, wall friction and interfacial shear stress dominate the film behaviour – a momentum equation can be dropped;
- wall temperature is below Leidenfrost point;
- the wavy surface of the film is modelled by a mean film thickness with a superimposed film roughness;
- the mean film surface is assumed to be parallel to the solid wall.

The above assumptions lead to an implementation of the wallfilm model as 2D finite volume method on the air flow wall boundaries.

Relevant physical effects that need to be taken into account are:

- interfacial shear force;
- gravitational acceleration;
- pressure gradient;
- film evaporation;
- heat transfer between film and wall and gas phase;
- interaction with impinging droplet spray;
- film entrainment.

The film thickness equation is the basic governing equation for the wallfilm flow. It represents slightly modified formulation of continuity equation where, instead of mass, wallfilm thickness is conserved property. The Cartesian formulation of the film thickness equation is:

$$\frac{\partial \delta}{\partial t} + \frac{\partial \delta u_1}{\partial x_1} + \frac{\partial \delta u_2}{\partial x_2} = \frac{1}{\rho A}(S_{mD} - S_{mV}) \qquad \textbf{(52)}$$

where δ is film thickness, ρ is density of the film, u_1 and u_2 are film velocity components, S_{mD} and S_{mV} are source terms and A is surface of the film.

If we assume that source terms are provided, equation (52) can be solved explicitly if velocity components are known. So, of primary interest is the method for determining the film velocity components.

The mean film velocity necessary for the film thickness equation is:

$$\bar{u}_L = \frac{\delta}{6\mu}\left[2\delta\left(\rho g - \frac{dp}{dx}\right) + 3\tau_{\mathrm{I}}\right] \qquad \textbf{(53)}$$

for laminar flow and:

$$\bar{u}_T = \frac{49}{594}\left(\frac{\delta}{\nu}\right)^{4/7} \cdot \frac{7\delta\left(\rho g - \frac{dp}{dx}\right) + 9\tau_I}{\rho^{11/14}\left(\rho g\delta - \frac{dp}{dx}\delta + \tau_I\right)^{3/14}} \quad \textbf{(54)}$$

for turbulent flow. ν is kinematic viscosity of film and dp/dx is a pressure gradient. As can be seen, film velocity is dependent on the effective shear stress τ_I at the phase interface. This shear stress is exactly the same as the stress which causes frictional resistance to the air flow τ_w. Since the mean film velocity is just a few percentage of the mean air velocity, the problem of film-air phase interaction reduces to a calculation of flow over rough walls. It is important to emphasize that film roughness has to be described properly. From the logarithmic law of the wall the wallfilm shear is calculated as follows:

$$\tau_w = \rho u^2 \left[\frac{1}{\kappa} ln\left(\frac{y}{\nu}\sqrt{\frac{\tau_w}{\rho}}\right) + C\right]^{-2} \quad \textbf{(55)}$$

Equation (55) has to be solved iteratively which costs most of the CPU time in wallfilm module. For values of $y+$ lower than 11.06, the linear profile of the laminar sublayer is used. Then the wallfilm shear is explicitly evaluated as:

$$\tau_w = \mu \frac{u_{//}}{d_{zp}} \quad \textbf{(56)}$$

C is constant dependent of the level of roughness which is defined using the Reynolds number for roughness:

$$Re_{ks} = \frac{k_s u_\tau}{\nu} \quad \textbf{(57)}$$

where k_s is the equivalent sand grain roughness determined as follows:

$$k_s = \psi_\tau(\tau_w) \cdot 2\delta \quad \textbf{(58)}$$

$$\psi_\tau = 0.1\left[ln(\tau_w + 2) + 0.022\tau_w + 6.57\right] \quad \textbf{(59)}$$

Using the Reynolds number for roughness three different regions of roughness effect with corresponding constant C are distinguished:

1. hydraulically smooth region $Re_{ks} \leq 5$:

$$C = 5.2 \quad \textbf{(60)}$$

2. transition region $5 < Re_{ks} \leq 70$:

$$C = 5.4494 + \left(3.0506 - \frac{1}{\kappa} ln\, Re_{ks}\right) \cdot sin\left[0.595 \cdot (\ln Re_{ks} - 1.61)\right] \quad \textbf{(61)}$$

3. completely rough region $Re_{ks} > 70$

$$C = 8.5 - \frac{1}{\kappa} ln\, Re_{ks} \quad \textbf{(62)}$$

Finally, we have all necessary relations for evaluation of wallfilm thickness equation. The iterative loop starts with initial value of τ_{w0} and sets up first approximation for k_s and Re_{ks}. Then C is evaluated and an updated value for τ_w is calculated from equation (55) where the old value for τ_w is used on the right side of equation. The procedure is repeated until τ_w converges sufficiently. Finally, film velocity components are evaluated using converged τ_w value and the film thickness equation is explicitly solved.

3. SPRAY CALIBRATION

To evaluate the influence of varying parameters in the main simulation, well-known spray parameters as an initial condition are essential for a CFD simulation. Spray calibration procedure consists of the following steps:

- determination of the start velocity, i.e. velocity of spray droplets on the nozzle exit;
- determination of the direction of injection of nozzle orifices and the angle of spray plumes;
- specification of the initial particle size distribution.

The single calibration steps of spray were verified with digital CCD (charge-coupled device) camera images, patternator measurements and laser light scattering measurements.

3.1. Experimental setup

For the investigations, a six-hole injector (200 μm hole diameter) made by Emitec type EM-A1.3 was used. The experiments were conducted using a water temperature of 25°C. Water was injected at a relative pressure of 8 bar into quiescent air temperature of 20°C vertically from above the test chamber where injector was mounted. The cycle time was 100 ms. In order to achieve the desired flow rates, namely 2.5 and 5 kg/h, opening and closing times of injector needle were changed with a frequency generator Rigol DG1022 which was connected to the injector via an amplifier.

3.1.1. Spray propagation

Visualization of spray behaviour inside the test chamber was performed using the AVL VisioScope which is a fully digital, triggerable video system especially designed for IC engine research. It is used to observe periodic phenomena in IC engines using a strobe. The images delivered by a digital CCD Camera are transmitted straight to the PC as digital data (and therefore with no loss of quality). A charge-coupled device (CCD) is a device for the movement of electrical charge, usually from within the device to an area where the charge can be manipulated, for in this case conversion into a digital value. Figure 9 depicts visualization of water spray propagation.

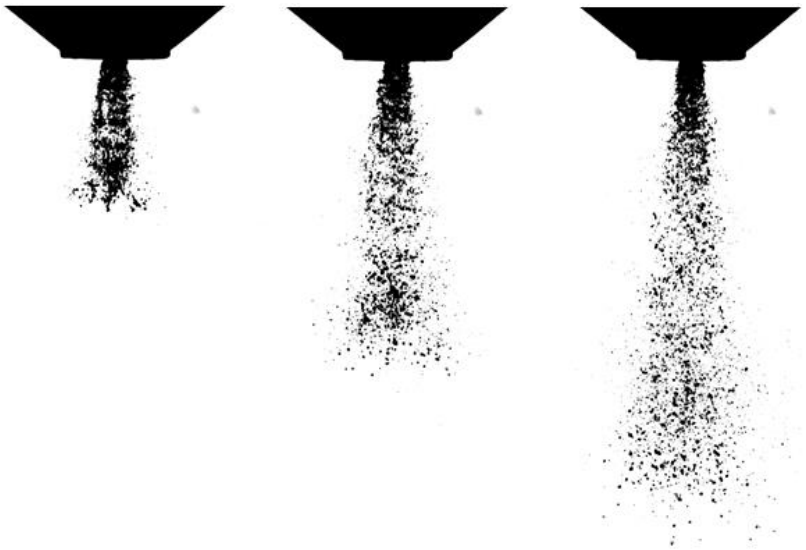

Figure 9. Visualization of spray propagation using VisioScope

3.1.2. Spray pattern

The so called spray pattern represents the spatial distribution of liquid mass on a plain perpendicular to the spray axis, measured at a fixed distance from the nozzle. It is important in a wide variety of applications. For example, in gas turbine combustors, variations in the local spray mass can cause fuel rich or fuel lean pockets, leading to increased pollutant emissions. Patternation of sprays is also important for numerical and theoretical model validation.

The device for measuring the spray pattern is conveniently called the patternator. In our case it consisted of 61 tubes (d=5.25 mm) whose arrangement is presented in Figure 10. Measuring procedure consists of positioning the patternator on different distances from the nozzle, perpendicular to the spray axis. Injected liquid is captured by the patternator tubes and by analysing amount of liquid collected in each tube we are able to deduce spray mass distribution on a given distance. Of course, this is just approximate distribution because we have a few error sources:

- part of the injected liquid passes through hollows between patternator tubes;
- patternator resolution i.e. number and diameter of tubes also affects the results – greater number of smaller tubes provides better approximation to real mass distribution;

- also, tubes wall influence shouldn't be neglected because it affects mass distribution by interacting with injected liquid.

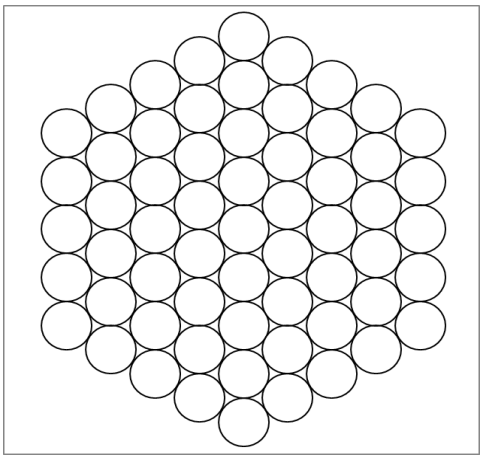

Figure 10. Arrangement of patternator tubes

Figure 11 depicts an example of a measured spray pattern obtained on various nozzle distances. As can be expected, evolution of spray through various physical mechanisms (primary and secondary break-up, deceleration due to aerodynamic forces, etc.) leads to a more uniform mass distribution as the distance from the nozzle increases.

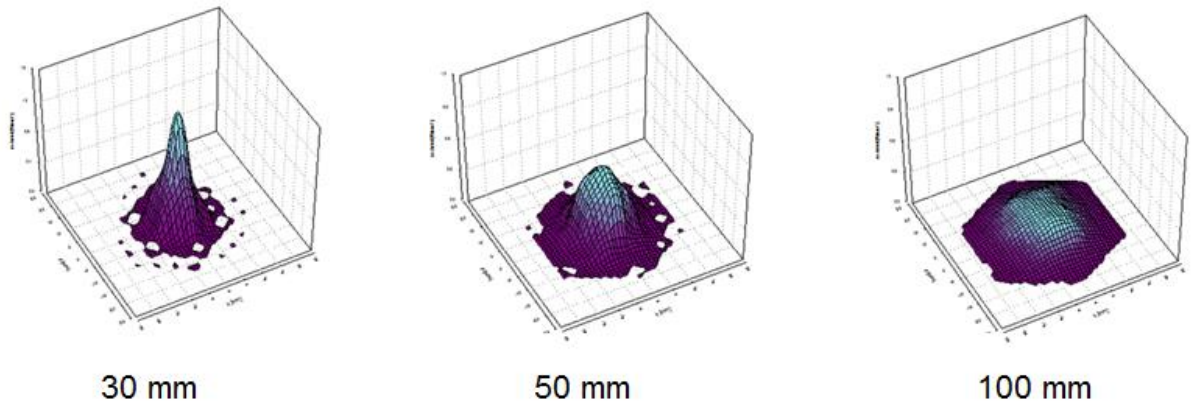

Figure 11. Spray mass distribution on different nozzle distances

In this work, patternator data from experimental injector was used for the determination of the injection direction of nozzle orifices and the angle of spray plumes. First, experimental data were recalculated in a form more suitable for comparison with simulation results. Accumulated liquid mass in each tube was converted into a liquid height using tube diameter and density at operating temperature:

$$h = \frac{m}{\rho \frac{d_t^2}{4} \pi} \tag{63}$$

Figure 12 shows recalculated data according to described procedure. It can be seen that, although liquid is injected into quiescent air, real spray is not symmetric. So, even before analyzing simulation results, we can expect discrepancies since numerical procedure yields symmetrical result.

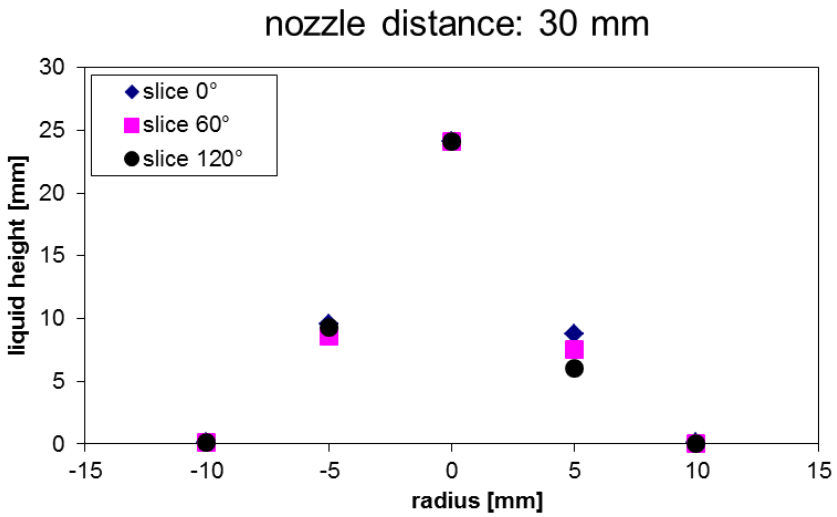

Figure 12. Example of recalculated experimental data

3.1.3. Particle size distribution

Commercial CFD code Fire is capable of predicting liquid spray evolution by taking into account phenomena such as secondary break-up and evaporation of liquid droplets. Furthermore, it is also equipped with primary break-up model that predicts initial particle (droplet) size distribution. However, this primary break-up model was developed for operating conditions that are different than those of the SCR application – high injection pressures and operating temperatures, so it cannot be utilized. Solution to this problem consists in initializing the calculation by specifying an initial particle size distribution obtained by modification of measured one [24].

The Spraytec instrument was used to measure the size of particles in a spray. Specifically, it measures the distribution of different sizes within a spray with a laser diffraction technique. The measurement process involves the following steps [25]:

1. A spray is prepared and delivered using an appropriate spray delivery device or accessory.

2. The spray is delivered between the two functional modules of the instrument, the transmitter and Receiver modules.
3. The Transmitter uses a He-Ne (Helium-Neon) laser to produce a laser beam that passes through the spray delivered to the measurement zone.
4. Detecting optics in the Receiver module detects the light diffraction pattern produced by the spray, converting the light detected into electrical signals. The signals are processed by analogue and digital electronics boards, and passed to the analysis software.
5. The light diffraction pattern is analysed using an appropriate scattering model to calculate the spray size distribution.
6. The software displays the results in a number of forms, including histograms, result-under plot and result-over plot, etc.
7. The user further processes the data as required.

3.2. Numerical simulation

Numerical simulations of the spray processes have been based on the Lagrangian multiphase model implemented in the CFD code FIRE as described in a previous section. Two mass flows, namely 2.5 and 5 kg/h have been used for the simulation cases. The simulation domain with relevant boundary conditions is shown in Figure 13. A three dimensional computational mesh with dimensions of 35 x 35 x 60 mm with 73 500 orthogonal hexahedron cells was used for the simulations.

Wall boundary conditions were defined on the top and bottom of the domain, while static pressure outlet was imposed at sides. In Fire, nozzle is defined as a point somewhere in the domain and is described by set of parameters given in so called nozzle file. The domain pressure and temperature were initialized according to the experimental data. First, the water was used for simulation cases and afterwards spray parameters were tuned up using AdBlue. Here will be presented final spray parameters obtained with AdBlue since they are used as an input in the next simulation. Although experiments were carried out with water, we can use them as a basis for AdBlue simulations since the differences in behaviour between the AdBlue and water is not so significant at low operating temperatures that prevailed in the experiment.

Pressure velocity coupling of momentum and continuity equation was obtained using the SIMPLE/PISO algorithm. The central difference discretization scheme was used for the convective term in the continuity equation with a blending factor of 1, while a MINMOD Relaxed with a blending factor of 0.5 was used for the convective terms in the momentum equations. Turbulence was modelled using advanced k-zeta-f model.

The time discretization varied, depending on the type of simulation and optimum (experience based) value between required computational time and satisfactory accuracy. In the case of spray penetration simulation the smallest step size of 10^{-5} s was used since the beginning of spray injection is highly transient process. For patternator simulation time step size of 1 ms was chosen and for PSD simulation 0.1 ms yielded satisfactory results. The droplet evaporation was determined by summing evaporation behavior of the single, isolated droplet dynamics inserted into gas flow, as described in previous chapter.

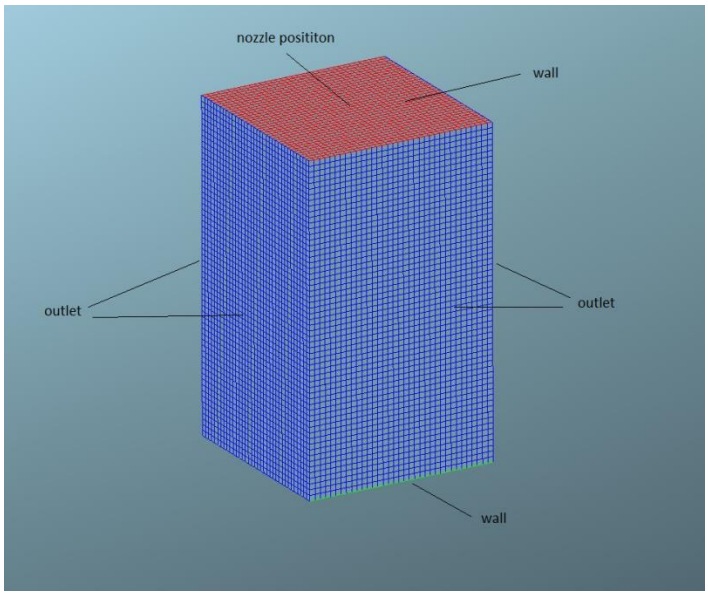

Figure 13. Computational domain for spray calibration

3.2.1. Spray penetration

This section describes simulations carried out in order to determine start velocity of spray. In Fire start velocity can be specified by some function, table or it can be set as constant. Relatively low injection pressure of 8 bar enables the usage of constant start velocity. Experimental data of spray penetration as a function of time were extracted from VisioScope measurements.

Figures below show comparison of measured and calculated results for both mass flows in the case of AdBlue as an injected liquid. It can be seen that spray penetration curves

have almost linear profile. There is only the indication of expected saturation on the end of curves. This is the consequence of high velocities, big droplets and relatively small test chamber so that aerodynamic forces due to relative velocity between droplets and air cannot significantly slow down spray droplets and yield more familiar spray penetration profile.

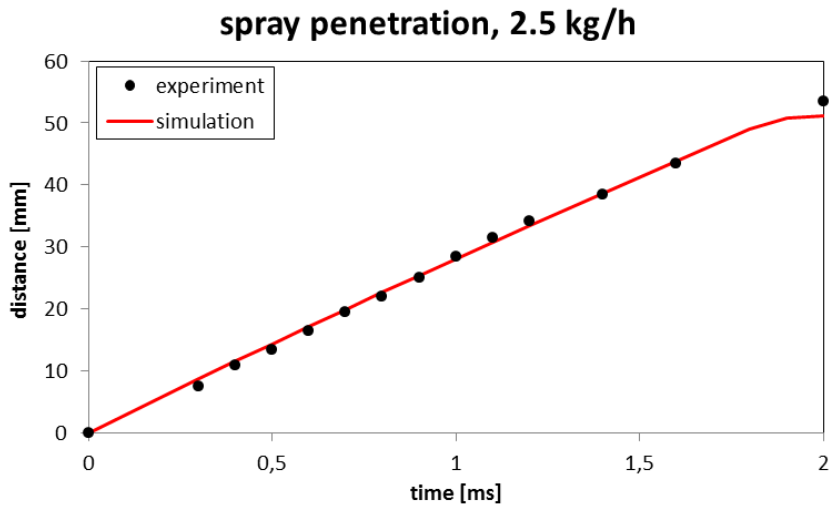

Figure 14. Spray penetration for mass flow of 2.5 kg/h

Despite the fact that experiments were carried out with water there was no much difference between penetration of AdBlue and water spray. In the case of water the best agreement with experimental results was achieved by setting the start velocity on 29 m/s for a both injection mass flows, 2.5 and 5 kg/h. These values should be corrected to 29.8 and 30 m/s in the case of AdBlue. By comparison of Figures 14 and 15 it can be seen that spray penetration exhibits very similar behaviour for both mass flows. This is expected since all operating conditions were the same for both mass flows and only the injector needle opening time was varied.

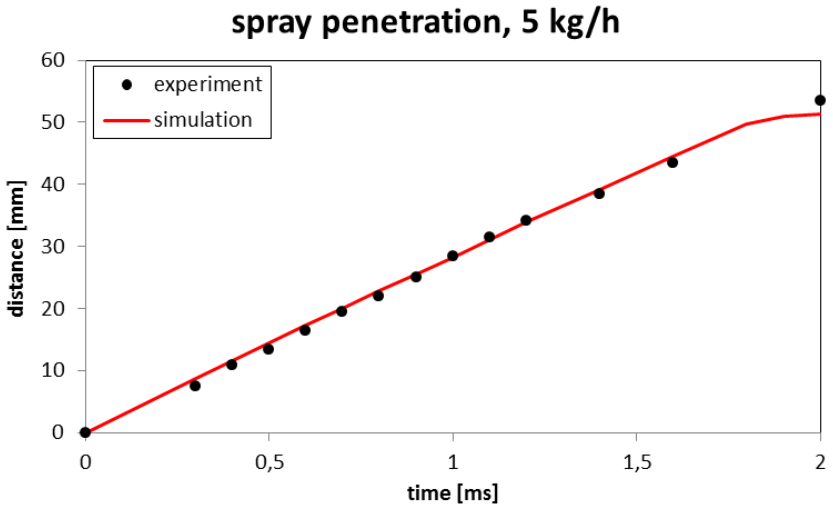

Figure 15. Spray penetration for mass flow of 5 kg/h

3.2.2. Spray pattern

The injection direction of nozzle orifices and the angle of spray plumes were varied in numerical simulation in order to match the spray pattern obtained by patternator measurement. Simulation set-up was slightly different than that of spray penetration. The known mass from patternator measurements was injected in one cycle during the time of 1 s because mass flow doesn't affect spray pattern. Hence, results that will be presented are equally valid for both mass flows. Furthermore, for this analysis 4 new meshes were created that had the same boundary conditions as previously described mesh. The only difference is their dimension and cell size. Reason for this lays in the way that spray pattern was determined.

Procedure of extracting required data (spray pattern) for comparison with experimental results consisted of the following steps:

- first, the plane parallel to the bottom wall of the test chamber was created in the middle of the last cell row;
- since the wallfilm module was deactivated, created plan was used as a tool for extracting and analysing pattern of liquid mass accumulated on the bottom wall (Figure 16); so it can be seen that we need meshes of different dimensions that correspond to different nozzle distances for which experimental data are given, namely 30 and 50 mm;
- numerical model of spray is based on certain simplifications that result in symmetric spray which has not been confirmed experimentally – this fact allows using data from

any of spray slice since they are all identical (first source of discrepancies as explained in spray pattern section);

- extracted data are converted into a liquid film height by using equation (1), except in this case the base is not circle, but square (because cells are hexahedrons).

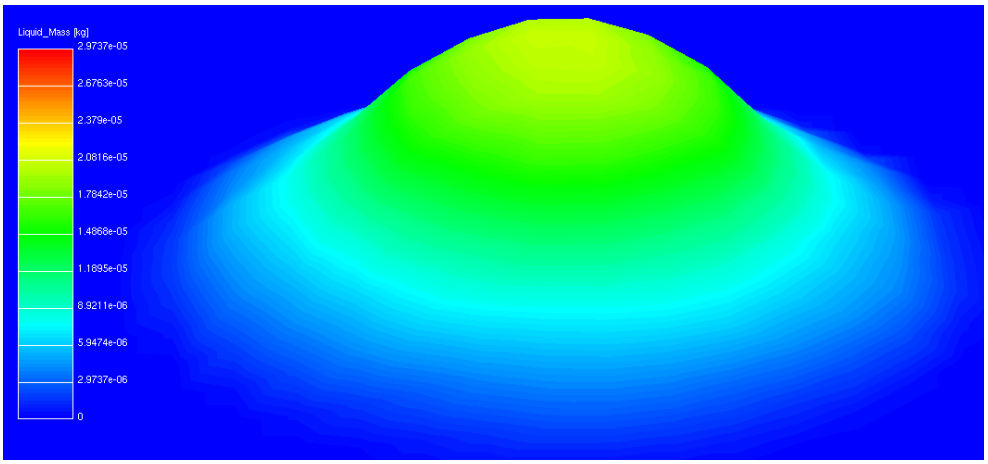

Figure 16. Example of simulated spray pattern

The following figures present results of parametric study which preceded the comparison with patternator measurements. In the legend first angle indicates orifice inclination, while the second one indicates angle of spray plumes. First, injection direction of nozzle orifices was kept constant while angle of spray plumes was varied.

As can be seen on Figure 17, angle of spray plumes has a decisive impact on both the area covered by the spray and mass distribution. At 5° inner halves of spray plumes are close to each other and contribute significantly to mass accumulated near the nozzle axis (black curve). By increasing that value plumes are separated, mass is more evenly distributed and spray covers larger surface.

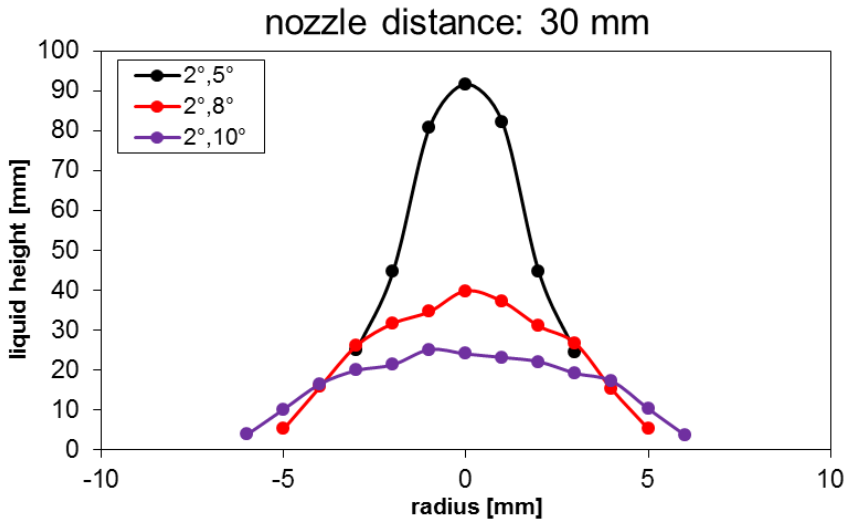

Figure 17. Results at constant injection direction of nozzle orifices

Figure 18 shows that varying the injection direction of nozzle orifices at a constant angle of spray plumes doesn't affect mass distribution very much. The area occupied by the spray remains the same and only the shape of mass distribution is slightly changed.

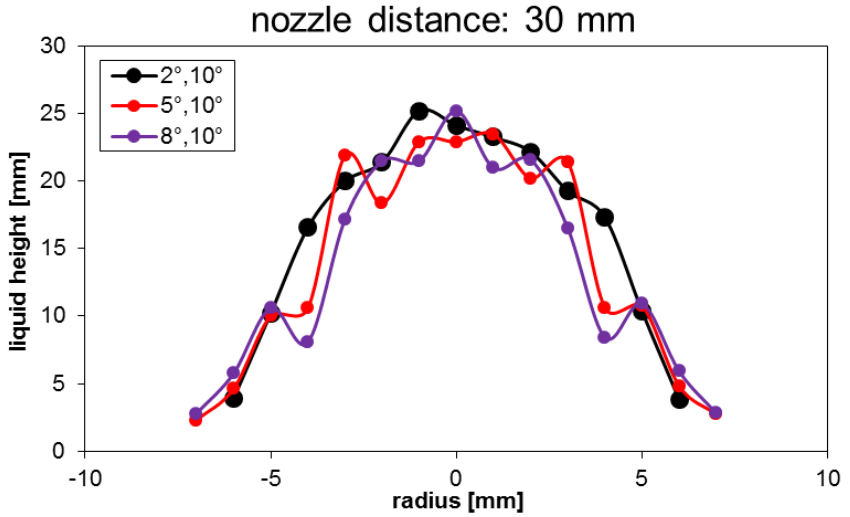

Figure 18. Results at constant spray plumes angle

Therefore, angle of spray plumes should be varied until the spray area is equal to that given in measurements. Afterwards, fine tuning of the injection direction of nozzle orifices provides close quantitative matching with experimental results.

On Figure 19 can be seen comparison of simulated results with experimental measurements for chosen set of angles that provided the best matching. Although some

oscillations are present on the simulated mass distribution, values on the locations for which measurement data are available, show close resemblance with the experiment.

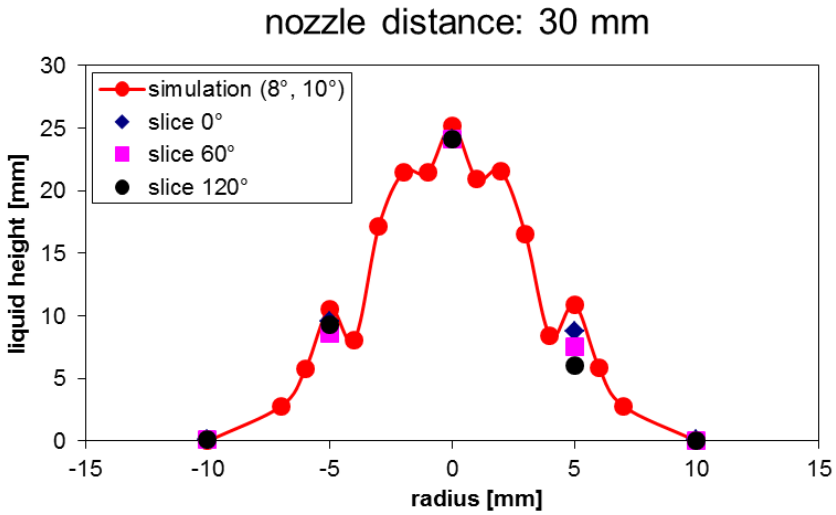

Figure 19. Comparison of simulated spray pattern with experiment

Before adoption of those values as final, we need to analyse impact of grid resolution on the results. As previously mentioned, diameter of patternator tubes is 5.25 mm. In simulations mesh cell size was 1 mm. Because of that there is a possibility that fine mesh won't capture injected liquid as patternator did, i.e. that the amount of mass captured by one of the patternator tubes will be distributed over a few mesh cells. Since for comparison with measurements we only used data from one cell on a given location, it is possible that simulated results, although match well with experiment, are wrong because larger area should be taken into account.

To investigate this possibility, simulation was started with optimum values of angles from Figure 19 on a coarser mesh whose cell size of 4 mm is closer to a patternator tube diameter. On Figure 20 we can see that the agreement with experimental results is not as good as in the case of finer mesh, so it can be concluded that the cell size has significant impact on results. Clearly, the chosen values of spray angle should be modified. Mass distribution exhibits the maximum deviation from the experiment in the nozzle axis and therefore the value of spray plumes angle should be decreased.

New set of values, namely the value of 8° for both angles, yields a very good agreement with measured data as can be seen on the figure below. Using results from coarse mesh might be counter-intuitive at a first sight but in this case is justified because cell size on a coarser mesh is comparable to patternator tube diameters.

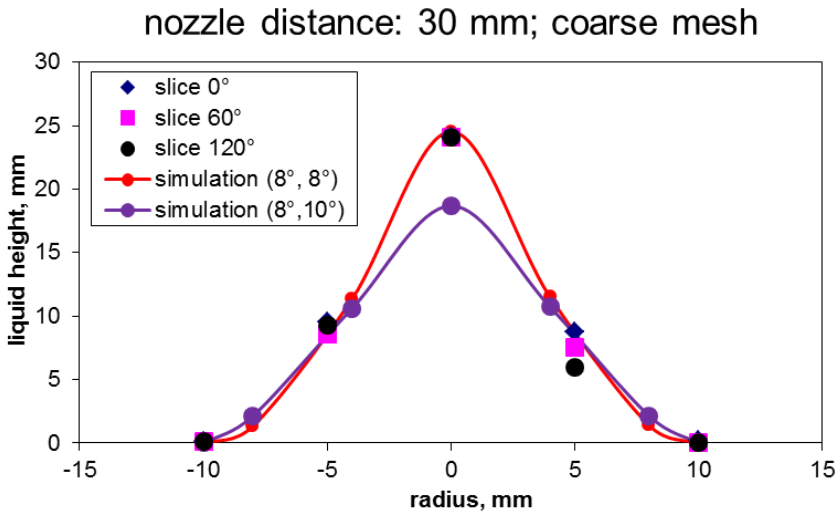

Figure 20. Spray pattern on a coarser mesh

Last check of the selected values is performed on the mesh that enables simulation of spray pattern on the nozzle distance of 50 mm. Agreement with experiment showed in the figure 21 is satisfactory although not so good as on the distance of 30 mm. Area occupied by the spray is larger and mass is more evenly distributed as is expected since the nozzle distance is increased.

With respect to all of the above, final values of spray angles are 8° for both the injection direction of nozzle orifices and the angle of spray plumes.

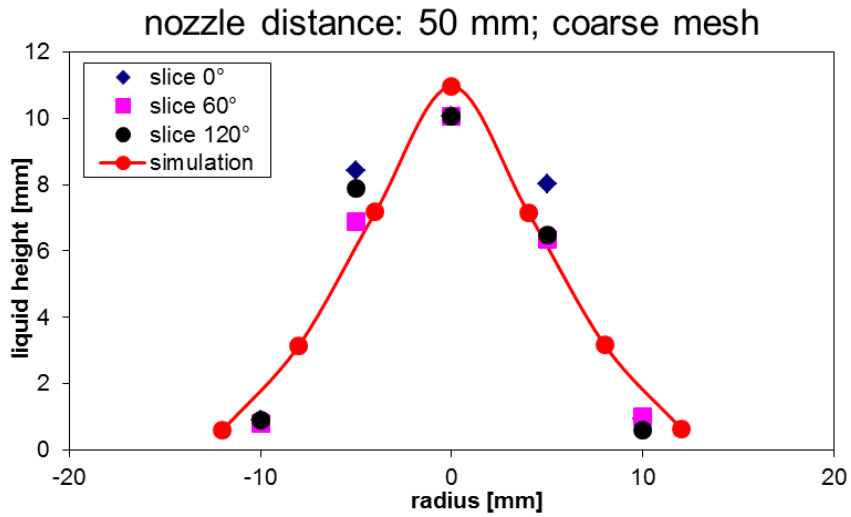

Figure 21. Spray pattern on the nozzle distance of 50 mm

3.2.3. Particle size distribution

Final step of spray calibration is determination of initial particle size distribution. This is the most important initial condition since primary break-up mechanisms implemented in Fire cannot be used for low injection pressures that prevail in SCR applications [24].

Initial particle size distribution is specified using experimental measurements on the distance of 30 mm. They are slightly modified, keeping that the integral of surface under the curve equals 1. Accuracy of the modified distribution for initializing the simulation is verified by comparing the extracted PSD curve on the distance of 30 mm from nozzle with the same experimental data that were basis for modified distribution. In order to obtain reliable average for comparison with experiment two injection cycles were simulated for each mass flow. Figures 22 and 23 show verification of chosen initial PSD curves. They present number based distributions. For visual clarity simulation results have been shown with markers, contrary to the convention.

Chosen input curves are confirmed by a good agreement between simulated and measured PSD at the distance of 30 mm. There are some deviations on the beginning of each curve but they can be attributed to error in experiment due to the curve flow at the beginning (vertical beginning which is nonphysical).

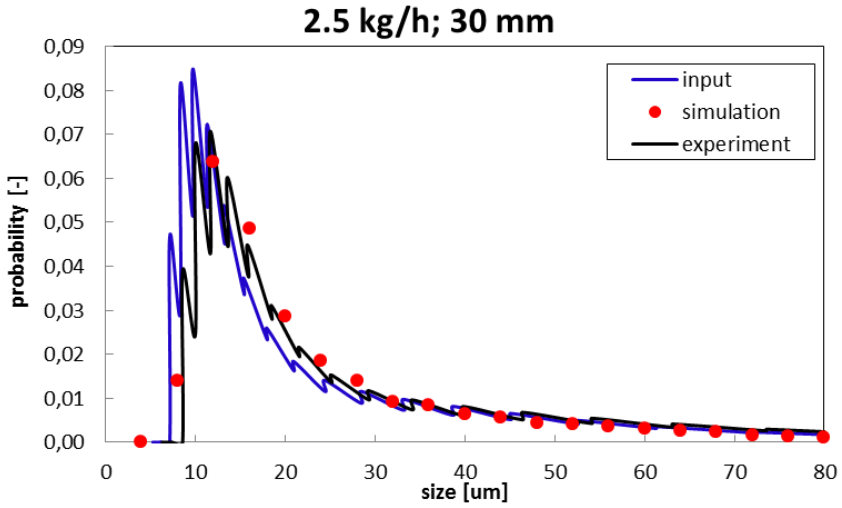

Figure 22. Number based droplet size distribution – 2.5 kg/h mass flow

Figure below shows that greater mass flows produces smaller drops. Higher injection speed and injected mass have a greater impact of aerodynamic forces as a consequence.

Stronger aerodynamic forces cause stronger break-up process and hence smaller average size of droplets.

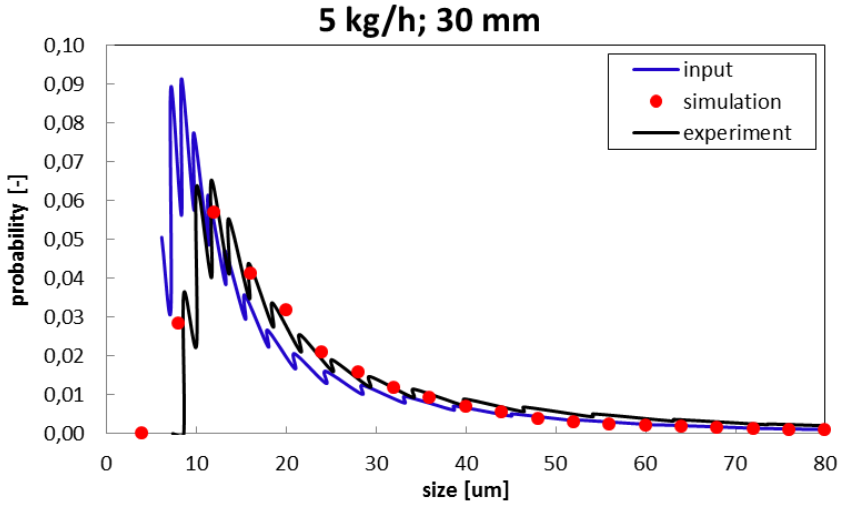

Figure 23. Number based droplet size distribution – 5 kg/h mass flow

Average Weber number was below 12, so according to Birkhold et al. [26] it appears reasonable to assume the absence of any secondary atomization process. Hence, the comparison on the larger distances from nozzle is not necessary. Furthermore, even if we look at larger distances there is no mechanism through which can modify distribution except specifying initial one which produces a good agreement on 30 mm.

3.3. Spray calibration summary

Final results of spray calibration are briefly summarized in the table below. D_{mean}, V_{lmean}, S_{mdt} and $D90$ are derived parameters that characterize each of the particle size distributions. It can be seen that the main difference between two mass flows is particle size distribution. Spray angles are identical as it was emphasized during the spray pattern determination procedure.

Table 1. Summary of spray calibration

Mass flow	2.5 kg/h	5 kg/h
Start velocity [m/s]	29.8	30
Injection direction of nozzle orifices [°]	8	8
Angle of spray plums [°]	8	8
D_{mean} [D10] [µm]	24.8	22.3
V_{lmean}[D30] [µm]	42.9	37.6
S_{mdt} [D32] [µm]	73.8	63.2
$D90$ [µm]	172	187

Finally, after quantitative establishment of all relevant spray parameters, figures below can serve as qualitative assessment of spray calibration. They represent comparison of simulated AdBlue spray propagation with experimental water spray. AdBlue spray is simulated with final calibration parameters and our assumption that because of low temperatures behaviour of AdBlue spray will be similar to that of water one is confirmed. This is not unexpected since AdBlue contains 67.5 % of water.

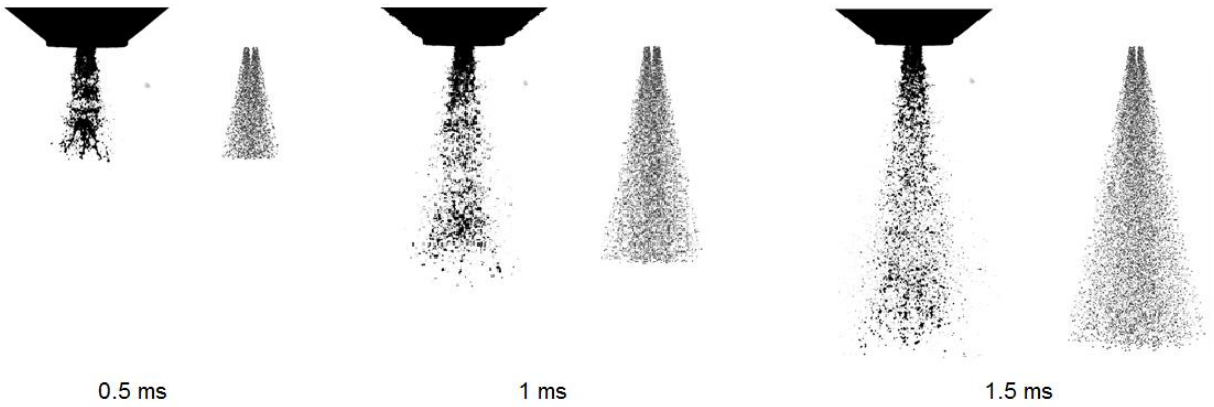

Figure 24. Comparison of spray penetration with CCD camera images, 2.5 kg/h

Comparison of Figures 24 and 25 shows that quantitatively there is no much difference in spray behaviour regarding different mass flows, since they look almost identically. Of course, particle size distributions are different but this cannot be determined by visual inspection.

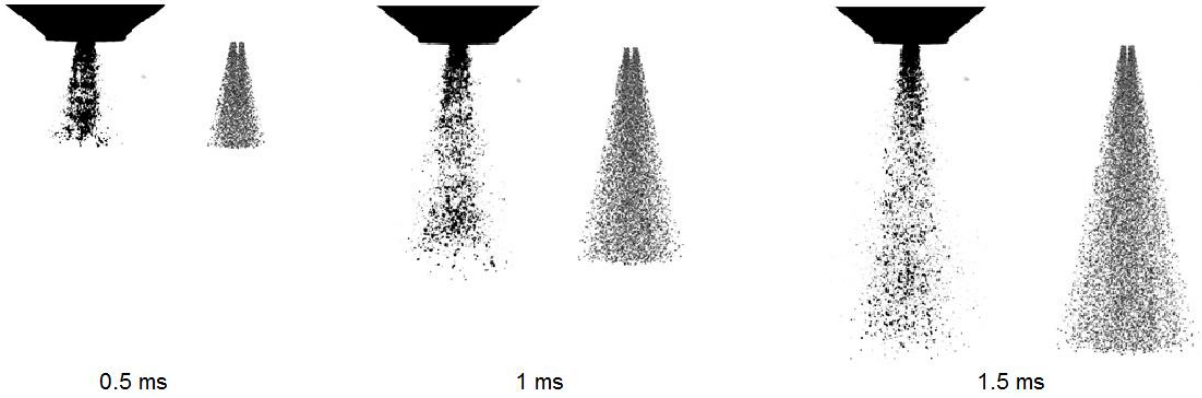

Figure 25. Comparison of spray penetration with CCD camera images, 5 kg/h

The next step is the SCR simulation which uses these calibration data for spray initialization. More details about main simulation are given in the next section.

4. MAIN SIMULATION

The object of this thesis is investigation of the spray interaction with the air stream and wall by means of numerical simulation and the validation of mathematical models integrated in commercial CFD code Fire. Spray parameters obtained in previous chapter are used as an input for the simulation of AdBlue spray injection into rectangular channel geometry.

4.1. Experimental setup

The test rig with a rectangular cross-section made of transparent and heat-resistant borosilicate glass was used for the analysis of wall film and air composition. It has dimensions of 970 x 120 x 45 mm and is available for optical measuring methods. Experiments were conducted with pure air. Figure 26 shows experimental set-up together with a CAD drawing with the appropriate dimensions of test section.

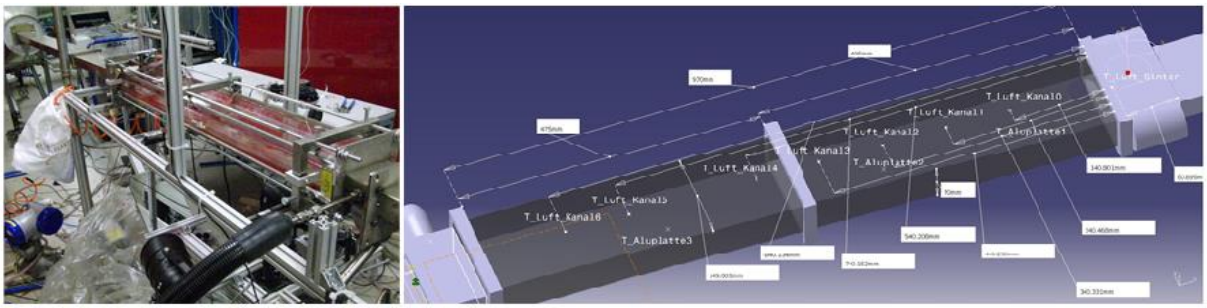

Figure 26. Test section and its CAD drawing with measuring points positions [27]

A six-hole injector made by Emitec, type EM-A1.3, was used for the introduction of AdBlue into the test section. The injector was located 40 mm after inlet into the test chamber and brought the liquid perpendicular to the inlet air stream (Figure 27). The operating pressure was 8 bar (gauge pressure) and duration of cycle time was 100 ms regardless of mass flow.

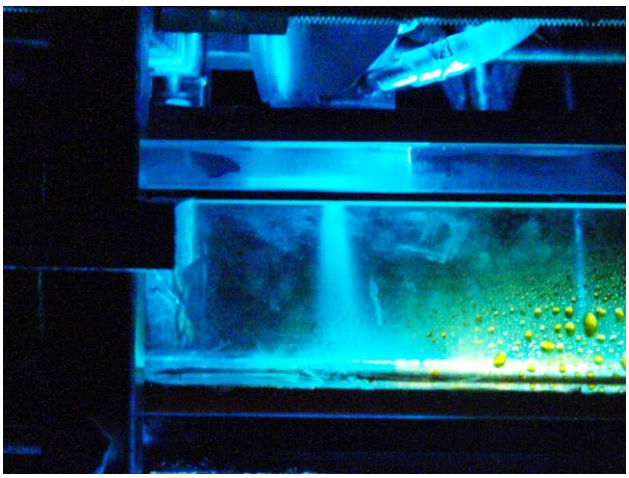

Figure 27. Injection of AdBlue in a test channel [27]

Figure 28 shows schematically one injection cycle. Higher mass flow of injected AdBlue was achieved by prolonging injection period, i.e. nozzle opening time, while maintaining the same injection cycle duration of 100 ms as well as all other operating conditions.

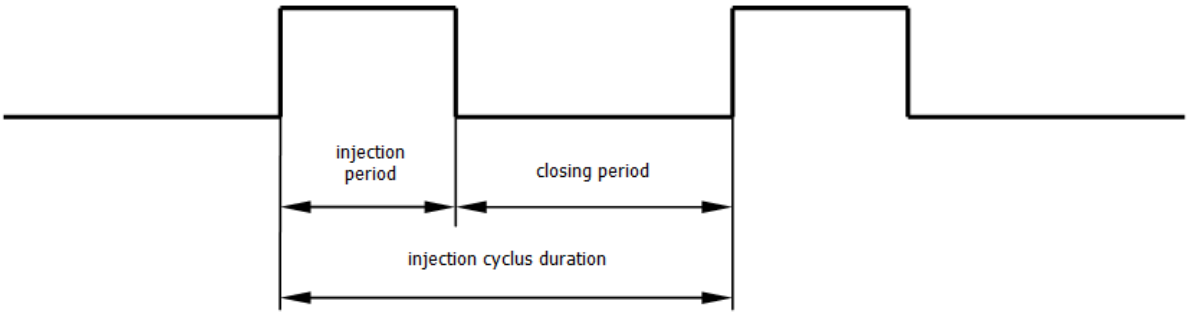

Figure 28. Representation of one injection cycle

To measure the mass flows reliably, the injector has been gauged in the following way: the flow rate was measured over a longer period while injector was at a frequency of 10 Hz, gauge pressure of 8 bar and at different injection periods. Obtained injection periods for the required flow rates are shown in the table below.

Table 2. Duration of injection period

Mass flow [kg/h]	Injection period [ms]
2,5	14,59
5	30,6

The wallfilm formation was investigated for different operating conditions with optical measuring methods. Cooling of the bottom plate has been recorded with an infrared camera. Furthermore, during each test, concentrations of ammonia and isocyanic acid formed during the urea thermolysis were determined at the outlet of the test chamber with Fourier transform infrared spectroscopy (FTIR). Sampling of air was conducted at nine points, which were evenly distributed across the channel cross section, on the height of 13, 18, 23 and 30 mm.

In the Fourier transform infrared spectroscopy, the molecules of a gas are excited with infrared radiation to oscillate and rotate. Each gas species have a characteristic band of absorbed wavelengths, which is linearly dependable to the concentration, so by observing absorbed infrared pattern, it can be found out not only about the gas composition but also about the exact concentration of each species.

4.2. Numerical simulation

Experiments carried out on the test section supplied data for numerical simulation of two cases whose parameters are given in a table below.

Table 3. Parameters of simulated cases

	Inlet air normal velocity [m/s]	Inlet air temperature [°C]	Injected AdBlue mass flow [kg/h]
Case 1	20	300	5
Case 2	20	400	2,5

The simulation domain with relevant boundary conditions is shown in Figure 29. A three dimensional computational mesh with dimensions of 970 x 120 x 45 mm with 335 280 hexahedron cells was used for the simulations. Mesh was refined in the vicinity of the nozzle in order to capture transient spray behavior. Also, boundary layer was created towards the bottom plate since wallfilm formation is expected to occur during the operation of injection.

Wall boundary conditions were defined on the domain sides, while static pressure outlet was imposed at the domain exit. Inlet was described with normal velocity, air temperature, turbulent kinetic energy and turbulent length scale. In Fire, nozzle is defined as a point somewhere in the computational domain and is described by set of parameters given in so called nozzle file. The domain pressure and temperature were initialized according to the experimental data.

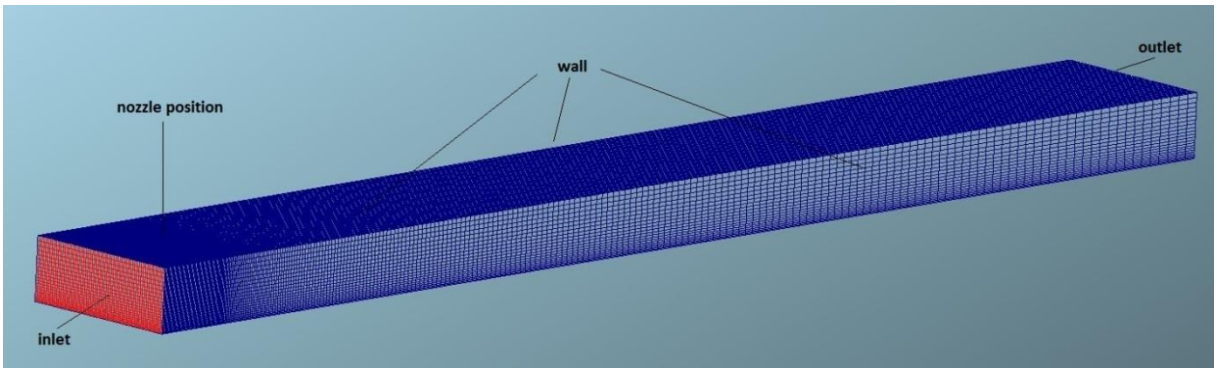

Figure 29. Computational domain with boundary conditions

Stationary temperature field of domain walls was important initial condition for simulation. It was obtained by carrying out steady state simulation with following settings:

- there was no injection of AdBlue;
- the same computational mesh was utilized;
- inlet air conditions are taken from experiment;
- convergence criteria of energy equation, namely normalized residual below 10^{-6}, was criterion for stationary state.

Obtained temperature fields are shown on a Figure below. It can be seen that they are identical in shape and only differ in magnitude. This is expected since two cases differ only in inlet air temperature while inlet velocity and turbulent quantities are the same.

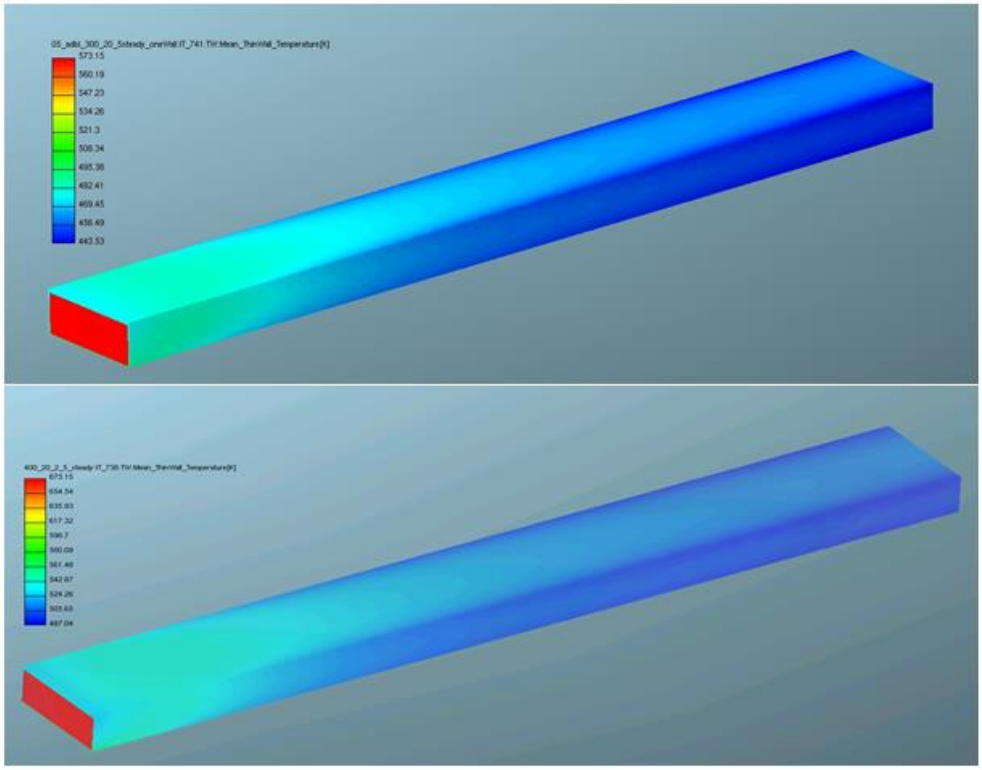

Figure 30. Wall temperature field – initial condition for Case 1 and Case 2

Pressure velocity coupling of momentum and continuity equation was obtained using the SIMPLE algorithm. The central difference discretization scheme was used for the convective term in the continuity equation with a blending factor of 1, while a MINMOD Relaxed with the same blending factor was used for the convective terms in the momentum equations. Turbulence was modelled using advanced k-zeta-f model.

The time discretization step of 1 ms was chosen on the basis of experience and represents optimum value between required computational time and satisfactory accuracy. The droplet evaporation was determined by summing evaporation behaviour of the single, isolated droplet dynamics inserted into gas flow, as described in chapter 2. Heat transfer through the wall is modelled with thin wall module which approximates the temperature profile of the wall with mean temperature. Heat loss towards the environment is modelled through the combined effect of convection and radiation. External heat transfer coefficient was set to 20 W/(m^2·K) which is a reasonable assumption for free convection in the environmental air. External wall emissivity was taken to be 0.3 and external air temperature was set to 293.15 K according to experiment.

4.3. Results

This section presents results obtained after 10 s of simulated time when quasi steady state was achieved. Postprocessor Impress gives results in form of species mass fractions, which need to be recalculated into mole fractions so that can be compared to experimental data. This was achieved by using the following expression:

$$y_i = \frac{x_i}{M_i \sum \frac{x_i}{M_i}} \tag{64}$$

where x_i is mass fraction of ith species, y_i is molar fraction of ith species and M_i is molar mass of ith species.

First, wallfilm development on the bottom plate presented on Figures 31 and 32 will be discussed. Experimental set-up was deliberately designed for wallfilm formation to appear in order that its effects on the main flow can be studied. Spray impingement causes local cooling of the wall. Deposition of droplets and wallfilm formation can occur if the surface temperature decreases below a critical value, i.e. if deposition or splashing regime occurs, as was described in chapter 2.

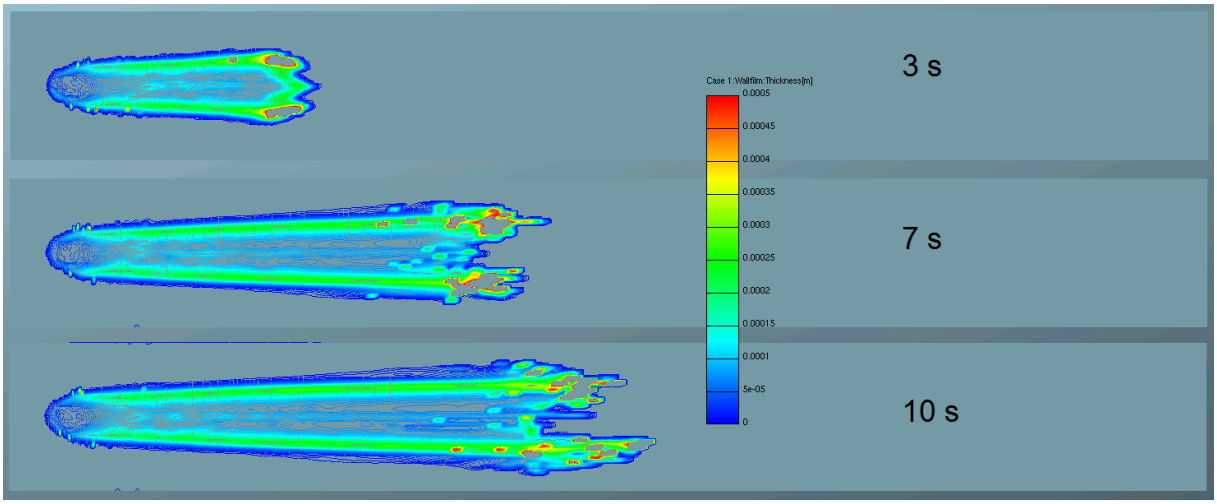

Figure 31. Case 1 - wallfilm development

In Figure 31 it can be seen that increase of surface covered with film gradually decreases with time. Increase in film area formed between 3rd and 7th second is larger than that formed between 7th and 10th second. Furthermore, after 10 s surface occupied by the wallfilm remains unchanged together with wallfilm shape, so it can be concluded that quasi steady state occurred. It cannot be spoken about stationary state since spray injection is highly

transient process. Most of the film mass is deposited in the peripheral parts of the film due to the influence of the main flow. Deposited liquid front of semi-circular shape propagates in the direction of the main flow and due to effect of viscosity leaves liquid trail behind. Average film thickness in those areas is between 200 and 250 μm.

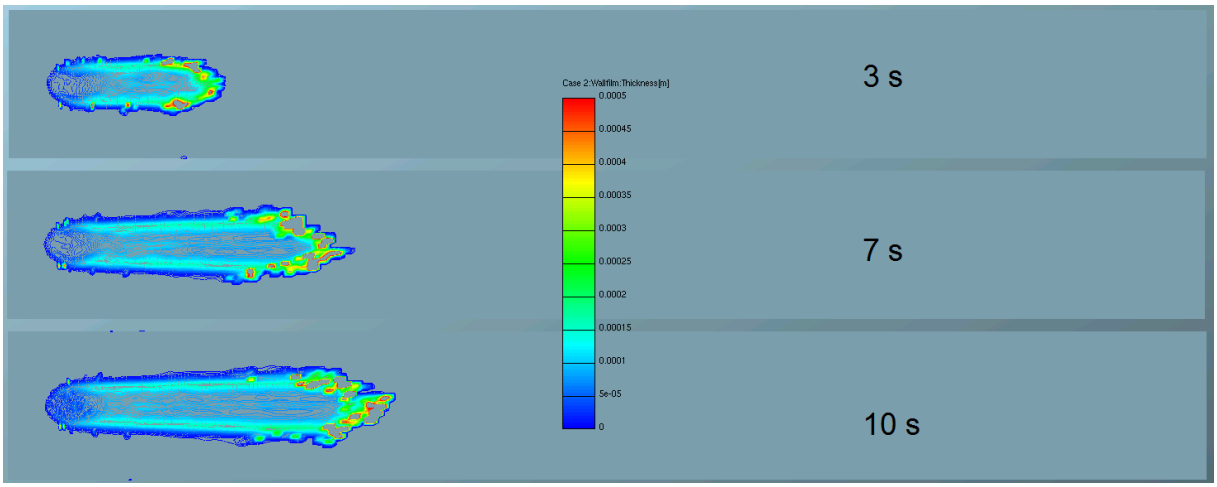

Figure 32. Case 2 - wallfilm development

Similar observations can be carried out also for case 2 shown in the Figure 32. The main difference is smaller film thickness, which is between 100 and 150 μm and smaller area covered with the wallfilm. Smaller mass flow of injected AdBlue together with higher air temperature causes stronger evaporation rates of the wallfilm and spray droplets as well as smaller deposits of AdBlue on the bottom plate.

In the experiment was observed great influence of the surface tension on the wallfilm formation that took place in the following manner:

- non-evaporated spray droplets impinging bottom plate decreased surface temperature in the region below the nozzle;
- after surface temperature decreased under critical value, wallfilm formation occurred;
- deposited liquid formed wallfilm in isolated area under the nozzle;
- at first, main flow couldn't drive the film along its direction due to effects of surface tension, so that isolated area of liquid deposition grew in thickness;
- after inertial effects due to accumulated mass prevailed over surface tension effects, abruption of the portion of wallfilm occurred;
- that portion was carried out downstream;
- described process was repeated periodically.

For better accuracy in describing effects of surface tension on the formation of wallfilm, wallfilm module incorporated in Fire must be supplemented with appropriate mathematical models.

It was mentioned earlier in the second chapter that thermal decomposition of urea occurs when all water from droplet evaporates, or in the case of wallfilm, when water mass fraction drops below 5%. Figure 33 represents mass fractions of H2O, NH3 and HNCO in central cross-section of computational domain after reaching the steady state. It can be seen that water mass fraction is low compared to ammonia and isocyanic acid. This is confirmation that urea thermolysis occurred in most part of the computational domain. On the same Figure can be seen that isocyanic mass fractions are higher than those of ammonia. Although this seems contradictory to equation (1) which says that in urea thermolysis equimolar amounts of ammonia and isocyanic acid are generated, it should be kept in mind that on Figure below mass fractions are presented and, because of higher molar mass of isocyanic acid, observed molar fraction will produce higher mass fraction. It needs to be checked by recalculating simulation data according to equation (64) whether simulation produced equimolar amounts of ammonia and isocyanic acid.

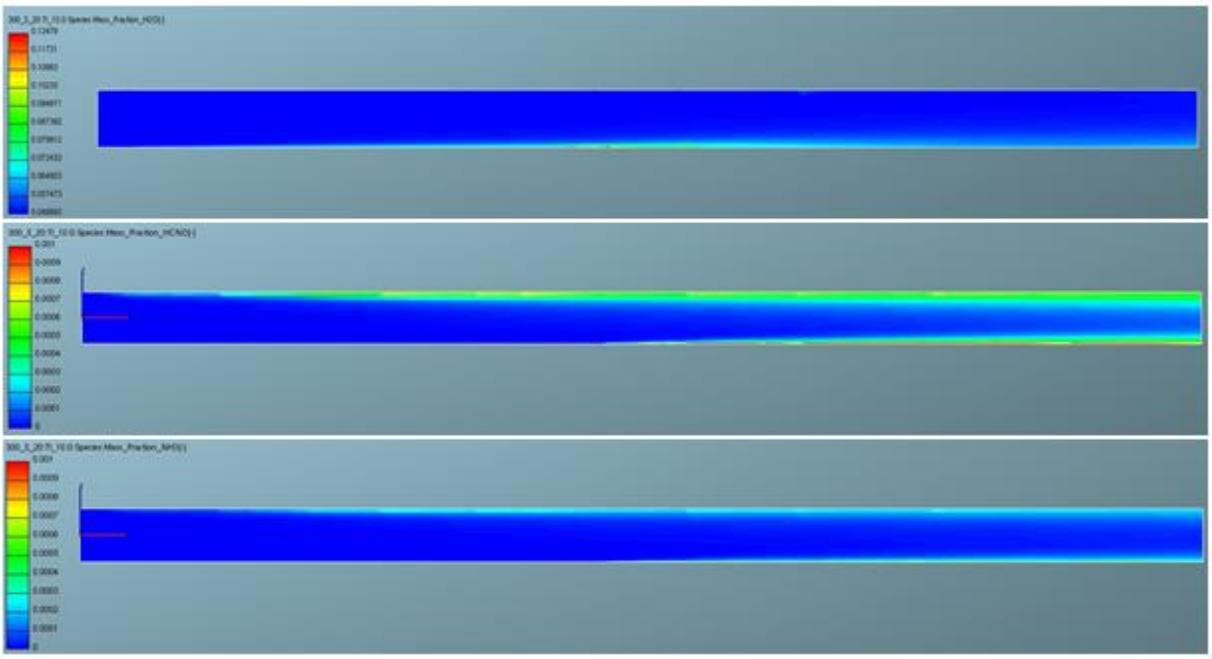

Figure 33. Concentrations of H_2O, HNCO and NH_3 – central cut

Sampling of air in the experiment was conducted on three equally spaced locations on each height. Average of species mole fraction on those three locations is given in experimental data for each height. Figure 34 shows distribution of HNCO on the domain exit.

Highest concentrations present in corners and near the edges of the domain impose question of physical mechanisms behind this distribution as well as how much discrepancies compared to experimental data will be introduced by averaging species mass fractions over all cells on each height.

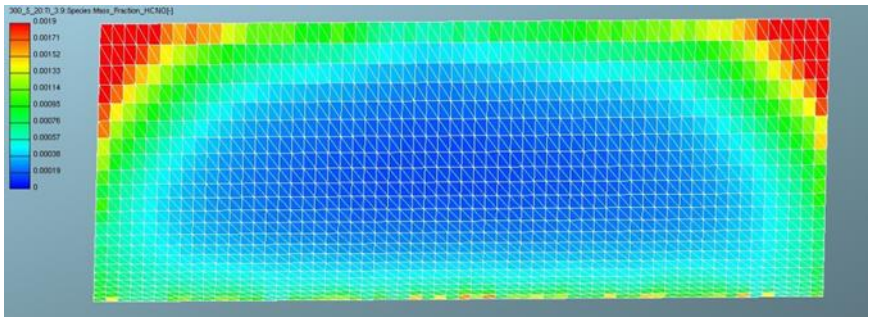

Figure 34. HNCO concentrations on the domain outlet

As for first question concerned, we need to perform thorough analysis of spatial distribution of HNCO (or NH_3 - since equimolar amounts are created by urea thermolysis it is not important which species we are analyzing) through the whole domain. In order to do so, spatial distribution of HNCO on perpendicular planes parallel to side wall and bottom wall on different distances are observed.

On Figure 35 it can be seen that HNCO mass fraction increases abruptly a few mm before side wall. Since flow is symmetric, the same is also valid for the other domain side.

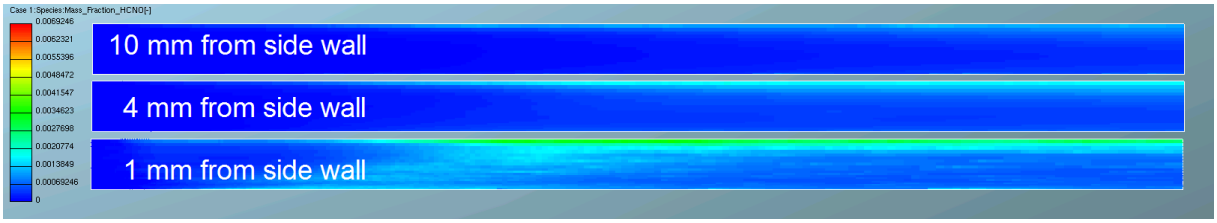

Figure 35. Plane cuts on different distances from side wall

Figure 36 shows even stronger increase in HNCO mass fraction near the upper wall. Such unexpected increase in concentration can be caused by spray/wall interaction or by intensive evaporation of spray droplets that are carried downstream of an injector.

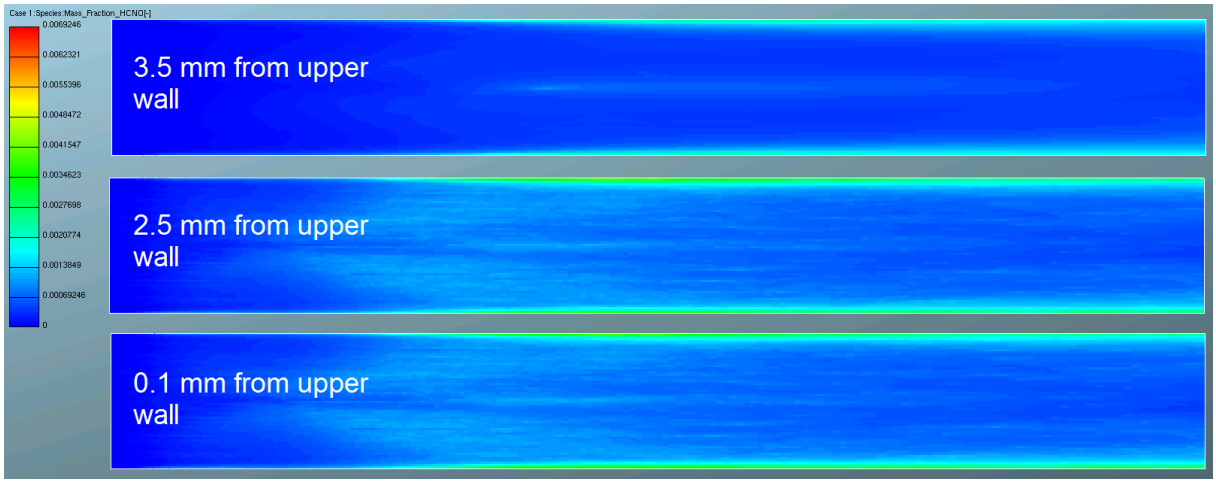

Figure 36. Plane cuts parallel with bottom plate

Surface cuts presented in Figure 37 confirm that increase in mass fraction of isocyanic acid is caused by spray/wall interactions. Small spray droplets are impinging on the hot wall surface and instantly evaporate and thermally decompose into ammonia and isocyanic acid. Since droplets are small, they cannot accumulate significant amount of heat from the walls and change their temperature. So, domain walls are thermal reservoir for impinging droplets. This is not the case for bottom wall because it is cooled by film of deposited liquid.

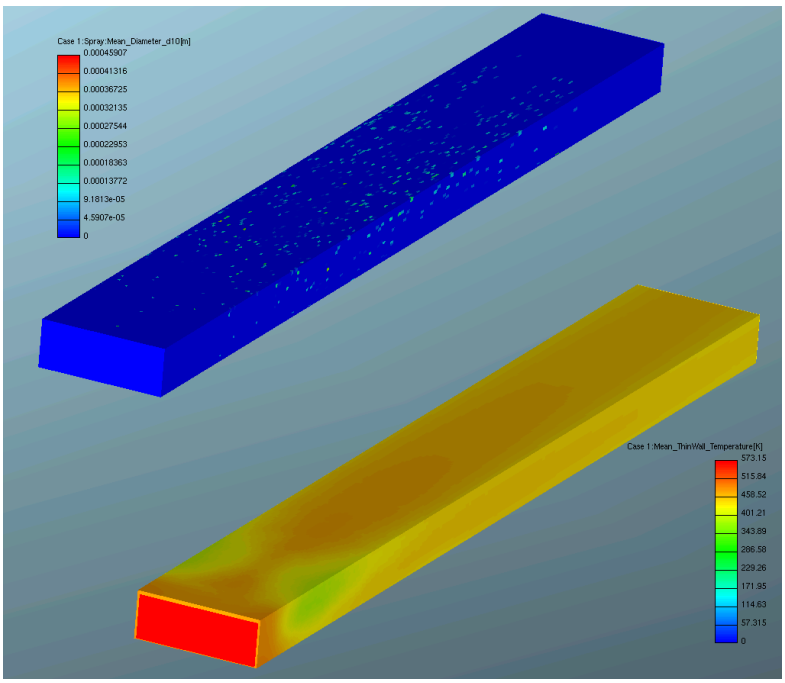

Figure 37. Surface cut - spray droplets impingement and wall temperature field

Higher concentrations of thermolysis products near the channel walls couldn't be captured in experiment because sampling locations weren't located in those regions. For this reason two cell rows on each side of the domain are excluded from averaging of species mass fractions obtained from simulation. Thus, large deviations from experimental results are avoided.

Final step of main simulation analysis is its validation with experimental data. Simulation results are recalculated according to equation (64). Following Figures show change in mole fractions of thermolysis products along channel height for both simulated cases. If we look just at the experimental results, there is no noticeable trend and higher concentrations of ammonia compared to concentrations of isocyanic acid in each case indicate that hydrolysis of isocyanic acid according to equation (2) occurred.

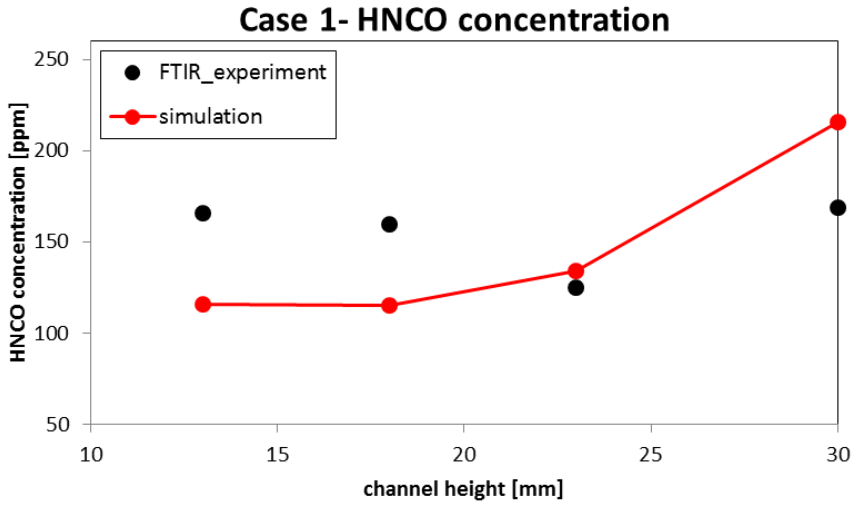

Figure 38. Comparison with experimental data; Case 1 – HNCO concentrations

Simulated results for case 1 show equimolar mass fractions of ammonia and isocyanic acid according to equation (1). Since hydrolysis of isocyanic acid wasn't modeled, there is higher deviation from experimental results in the case of ammonia concentrations shown in the Figure below. Although not excellent, agreement with experimental results is satisfactory. Higher mass flow of injected AdBlue in the first case, in spite of lower operating temperature, yields higher concentrations of thermolysis products compared to Case 2.

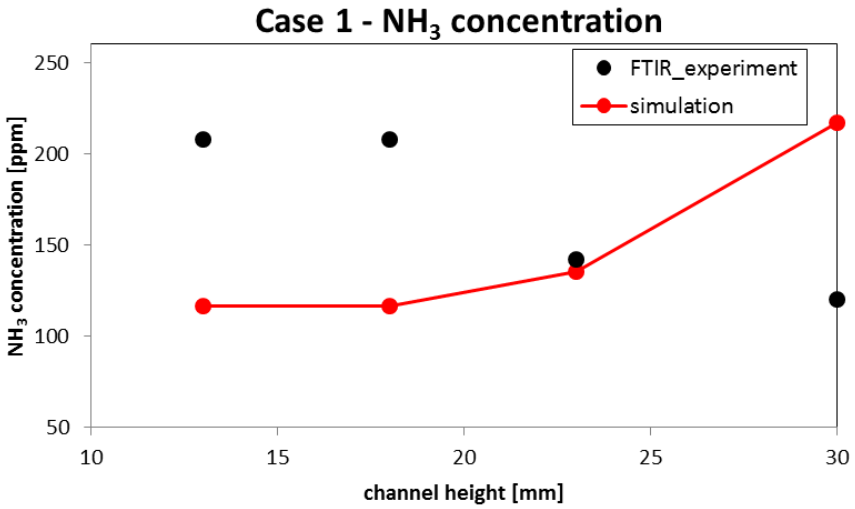

Figure 39. Comparison with experimental data; Case 1 – ammonia concentrations

Similar conclusions could be drawn also for the Case 2, although the deviation from the experiment is not so pronounced as in the first case.

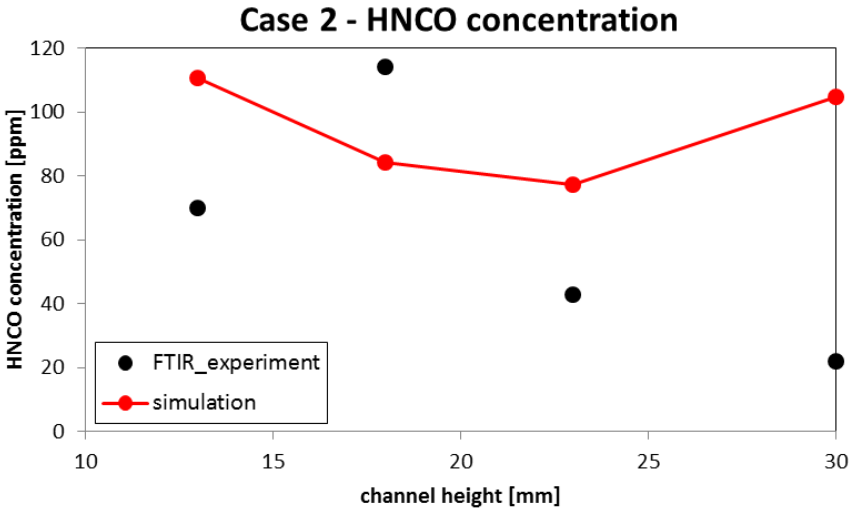

Figure 40. Comparison with experimental data; Case 2 – HNCO concentrations

There cannot be noticed some kind of concentration trend along channel height neither in experiment, nor in simulation. Shape and size of sampling port in experiment (ellipse with dimensions of major and minor axis of 10 and 8 mm) introduced additional uncertainty in measured results because of relatively large area which it encompass.

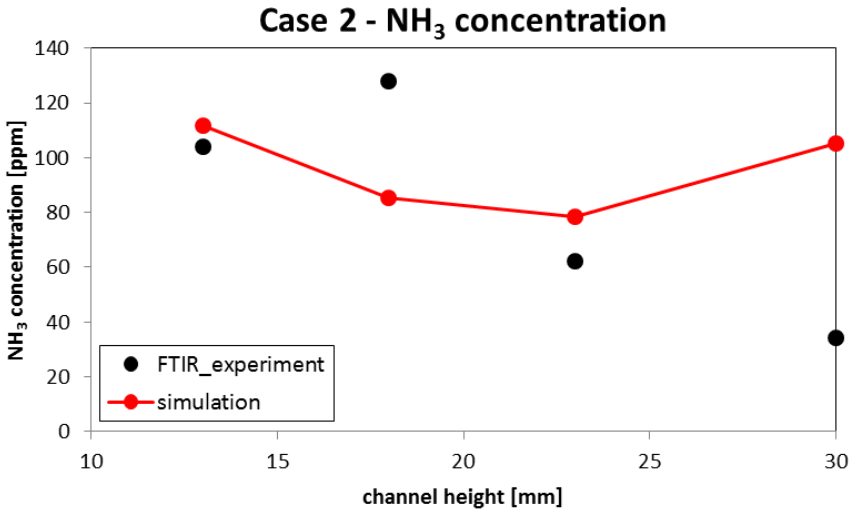

Figure 41. Comparison with experimental data; Case 2 – ammonia concentrations

In experiments were observed urea deposits and its chemical transforms whose modelling is extremely complicated because of underlying complex chemical behaviour which is not yet completely understood. In order to achieve better description of observed physical phenomena, mathematical models implemented in Fire should include:

- effects of surface tension on the formation of wallfilm;
- description of urea deposits.

5. CONCLUSION

In this thesis the investigation of the spray/wall interaction was carried out by means of numerical simulation in order to validate mathematical models integrated in commercial CFD code Fire. To predict the generation and distribution of the ammonia a detailed three-dimensional numerical simulation was performed. UWS droplets were treated with Lagrangian particle tracking, which solves the equations of motion, mass and enthalpy for parcels of droplets with identical properties. Deposition of droplets leads to the formation of a wallfilm which was modeled with a 2D finite volume method in the Fire wallfilm module.

The first objective was to determine spray parameters for the main CFD simulation since primary breakup of spray is still insufficiently understood. The single calibration steps of spray were verified with digital CCD (charge-coupled device) camera images, patternator measurements and laser light scattering measurements. The results were in a good agreement with the measured values for both mass flows that were analysed.

Data obtained from spray calibration served as an input for the main simulation where the spray/wall-interaction and wallfilm formation were investigated in a rectangular flow channel geometry. Obtained results show satisfactory agreement with experimental data, although there is larger deviation in case of ammonia mole fractions because hydrolysis of isocyanic acid wasn’t modelled in numerical simulations.

Within this work mathematical models regarding spray/wall interactions and wallfilm formation integrated in Fire CFD code have been proven as a valuable tool for the design and optimization of real mobile SCR systems.

It is important to note that further improvements can be made by extending the current model to include surface tension effects as well as simplified chemistry of urea deposits. The continuation of this work would also entail improved simulations that will include models for describing hydrolysis of isocyanic acid that are already available in Fire and re comparison with same experimental results to establish how much improvement is achieved with this modified approach.

REFERENCES

[1] http://en.wikipedia.org/wiki/European_emission_standards

[2] Kröcher, O., Elsener, M., Jacob, E., New reducing agents for the low NOx SCR technology, Proceedings of the 5th International Exhaust Gas and Particulate Emissions Forum, Ludwigsburg (Germany), pp. 98-119, 2008.

[3] Nishioka, A., Sukegawa, Y., Katogi, K., Mamada, H., Kowatari, T. A Study of a New Aftertreatment System (2): Control of Urea Solution Spray for Urea-SCR, SAE 2006-01-0644, 2006.

[4] Fang, H. L., DaCosta, H. F. M. Urea thermolysis and NOx reduction with and without SCR catalysts, Applied Caralysis B: Environmental, No. 46, pp. 17-34, 2003.

[5] Koebel, M., Elsener, M., Kleemann, M. Urea-SCR: a promising technique to reduce NOx emissions from automotive diesel engines, Catalysis Today, No. 59, pp. 335-345, 2000.

[6] Jacob, E. Perspectives on Mobile SCR Technology, 15th Aachen Colloquium, 2006.

[7] Kim, J. Y., Ryu, S. H., Ha, J. S. Numerical prediction on the characteristics of spray-induced mixing and thermal decomposition of urea solution in SCR system, In Proc. 2004 Fall Technical Conference of the ASME Internal Combustion Engine Division, Long Beach, California USA, 2004.

[8] Nguyen, T. D. B., Lim, Y., Eom, W. H., Kim, S. J., Yoo, K. S. Experiment and CFD simulation of hybrid SNCR–SCR using urea solution in a pilot-scale reactor, Computers and Chemical Engineering, Vol. 34, Issue 10, pp. 1580–1589, 2010.

[9] van Helden, R., Verbeek, R., Willems, F., van der Welle, R. Optimization of Urea SCR DeNOx Systems for HD Diesel Engines, SAE 2004-01-0154, 2004.

[10] Versteeg, H. K., Malalasekera, W. An Introduction to Computational Fluid Dynamics: The Finite Volume Method, 2nd Edition, Prentice Hall, 2007.

[11] Ferziger, J. H., Peric, M. Computational Methods for Fluid Dynamics, 3rd, rev. edition, Springer, 2002.

[12] Patankar S. V. Numerical heat transfer and fluid flow, Hemisphere Pub. Corp., 1980.

[13] Vujanović M.: Numerical modeling of multiphase flow in combustion of liquid fuel, PhD thesis, Faculty of Mechanical Engineering and Naval Architecture, University of Zagreb, Zagreb, 2010.

[14] AVL Fire: Lagrangian Multiphase Module Manual, version 2011

[15] Abramzon, B., Sirignano, W. A. Droplet vaporization model for spray combustion calculations, Int. J. Heat Mass Transfer, Vol. 32, No. 9, pp. 1605-1618, 1989.

[16] Dukowicz, J. K., Quasi-Steady Droplet Phase Change in the Presence of Convection, Informal Report, Los Alamos Scientific Laboratory, LA-7997-MS, 1979.

[17] Yuen, M. C., Chen, L.W., On drag of evaporating liquid droplets, Combust. Sci. Technol. 14, 1976, pp. 147-154

[18] Kontin, S., Höfler, A., Koch, R., Bauer, H. J. Heat and Mass Transfer accompanied by Crystallisation of single Particles containing Urea-water-solution, ILASS – Europe 2010, 23rd Annual Conference on Liquid Atomization and Spray Systems, Brno, Czech Republic, 2010.

[19] Musa, S. N. A., Saito, M., Furuhata, T., Arai, M. Evaporation Characteristics of a Single Aqueous Urea Solution Droplet, International Conference on Liquid Atomization and Spray Systems (ICLASS), 2006

[20] Wang, T. J., Baek, S.W., Lee, S.Y. Experimental Investigation on Evaporation of Urea-Water-Solution Droplet for SCR Applications, AIChE Journal, Vol. 55, No. 12, December 2009.

[21] Birkhold, F., Meingast, U., Wassermann, P., Deutschmann, O. Modeling and simulation of the injection of urea-water-solution for automotive SCR DeNOx-systems, Applied Catalysis B: Environmental, No. 70, pp. 119-127, 2007.

[22] Yim, S. D., Kim, S. J., Baik, J. H., Nam, I., Mok, Y. S., Lee, J. H., Cho, B. K., Oh, S. H. Decomposition of Urea into NH3 for the SCR Process, Industrial & Engineering Chemistry Research, 2004, 43, pp. 4856-4863, 2004.

[23] Mundo, C., Sommerfeld, M., Tropea, C. Droplet-Wall Collisions: Experimental Studies of the Defromation and Breakup Process, Int. J. Multiphase Flow, Vol. 21, No. 2, pp. 151-173, 1995.

[24] Gapin, A., Demoulin, F., Dumouchel, C., Pajot, K., Patte-Rouland, B., Réveillon, J. Development of an Initial Drop-Size Distribution Model and Introduction in a CFD Code to Predict Spray Evolution, 7th International Conference on Multiphase Flow ICMF 2010, Tampa, Florida, 2010.

[25] Malvern Instruments: Spraytec User Manual MAN0368, Issue 3.0, May 2007.

[26] Birkhold, F., Meingast, U., Wassermann, P. Analysis of the Injection of Urea-water-solution for automotive SCR DeNOx-Systems: Modeling of Two-phase Flow and Spray/Wall-Interaction, SAE 2006-01-0643, 2006.

[27] ViF Projekt B03-T01 (Experimentelle Untersuchungen zur Wandfilmbildung): K2-Endbericht ViF-ZB-08/2012, 2012.

APPENDICES

I. CD-R disc